Engineering Structures 312 (2024) 118244

Contents lists available at ScienceDirect

Engineering Structures

journal homepage: www.elsevier.com/locate/engstruct

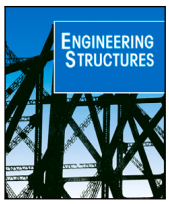

Analytical and numerical models to determine the strength of RC exterior beam–column joints retrofitted with UHPFRC

Ingrid Rocio Irreño Palomo [a], Giada Frappa [b,*], Luiz Carlos de Almeida [a], Leandro Mouta Trautwein [a], Margherita Pauletta [b]

[a] Faculty of Civil Engineering, Architecture and Urbanism, University of Campinas, CEP 13083-852, Campinas, SP, Brazil
[b] Polytechnic Department of Engineering and Architecture, University of Udine, Via delle Scienze, 206, 33100 Udine, Italy

ARTICLE INFO

Keywords:
Reinforced concrete
Exterior beam–column joints
Ultra-high-performance fiber reinforced concrete
Retrofit
Flexural model
Shear model
Numerical model
Experimental comparison

ABSTRACT

Analytical and numerical models are proposed to assess the strength of exterior Reinforced Concrete (RC) Beam–Column Joints (BCJs) retrofitted with Ultra-High-Performance Fiber Reinforced Concrete (UHPFRC) jacket subjected to cyclic lateral loads. In particular, an analytical flexural model is provided to calculate the flexural strength of the beam converging to the BCJ. The flexural model is also used to determine the shear force acting in the joint at beam flexural failure.

An analytical shear model to calculate the joints' shear strength is also proposed. This model considers the contributions to the joint strength of both the joint core and the UHPFRC jacket and takes also into account the confinement effect produced by the jacket on the joint core. The flexural and shear analytical models are validated through the comparison with experimental results available in the literature, showing high accuracy in the predictions. The finite element model of a BCJ retrofitted with HPFRC jacket for which experimental test results are available in the literature is also implemented. A solution to reproduce the interface interaction at the contact surface between concrete and UHPFRC is proposed. The numerical model shows good accuracy in predicting the joint experimental behavior.

1. Introduction

Earthquakes can cause severe damages to RC structures that are not appropriately designed to bear seismic forces, putting human lives at risk. Due to this, high interest in studying structural elements subjected to cyclic loads has increasingly developed in the last decades, particularly for beam–column joints, which are subjected to brittle failure if not adequately designed. Consequently, strengthening BCJs is fundamental for increasing the ductility of existing RC framed buildings, especially those built before the 1970s [1,2], which usually do not satisfy seismic requirements.

To avoid BCJs failure, diverse retrofit techniques have been developed, both for strengthening and structural repair, such as epoxy resin injections [3], RC jacketing [4], steel jacketing [5], and application of steel plates [6,7], steel braces [8] and fiber reinforced polymers [9–23]. In the last years, also High Performance Fiber Reinforced Concrete (HPFRC) and Ultra-High Performance Fiber Reinforced Concrete (UHPFRC) have been used for retrofitting beam–column joints [24–29], and also beams [30–40] and columns [41–44]. Due to their dense microstructure HPFRC and UHPFRC are expected to address the durability issue evidenced by conventional concrete. UHPFRC can be defined as a Ultra-High Performance Concrete (UHPC) with presence of fibers, with higher flowability than Self-Compacting Concrete (SCC), which reaches compressive strength values of at least 150 MPa [45–49]. On the other hand, HPFRC can be defined as a concrete with properties of High Strength Concrete (HSC) and a workability equivalent to that of SCC, reaching compressive strength values up to 200 MPa [50–53]. Regarding the tensile behavior, the main difference is that UHPFRC has higher tensile strength, due to the higher fiber volume (usually higher than 2%). Both HPFRC and UHPFRC develop hardening and microcracking, as it can be seen from the trilinear stress–strain tensile curve (elastic-hardening-softening branches) [30,46,47,54]. According to AFGC guidelines [48], UHPFRC is usually characterized by tensile strength values between 7–15 MPa.

French Building Code [49] describes UHPFRC as a material with high compressive strength and high post-cracking tensile strength, which produces ductile behavior in tension. Thanks to these properties, as retrofit material, UHPFRC provides the structural elements to which it is applied with higher energy absorption capacity, durability, flexural strength, and shear strength [45]. Several experimental studies on BCJs

* Corresponding author.
E-mail address: giada.frappa@uniud.it (G. Frappa).

https://doi.org/10.1016/j.engstruct.2024.118244
Received 9 November 2023; Received in revised form 18 April 2024; Accepted 17 May 2024
Available online 25 May 2024

retrofitted with HPFRC/UHPFRC jackets have been carried out in the last decades. Shannag et al. [24] and Shannag and Alhassan [25] investigated BCJs retrofitted with HPFRC jackets of thickness 15 mm and 25 mm. In the retrofitted joints the authors observed a ductile failure mode, enhancements in the load capacity, energy dissipation and ductility, and less stiffness degradation. Beschi et al. [26] investigated the effectiveness of a HPFRC jacket with thickness of 30 mm in the beam and 40 mm in the column as retrofit intervention for exterior non-seismic BCJs. The authors observed increases in the joint shear strength, lateral displacement capacity and energy dissipation capacity, and ductile flexural failure at the beam. Khan et al. [27] repaired exterior BCJs using 30 mm thick UHPFRC plates. The experimental tests' results showed improvements in the shear capacity, stiffness, energy dissipation capacity and ductility. Sharma and Bansal [28] retrofitted exterior BCJs with Ultra-High Performance Hybrid Fiber Reinforced Concrete (UHP-HFRC) jackets of thickness 25 mm, obtaining improvements in the load capacity, ductility, energy dissipation, and stiffness. Saharan et al. [29] retrofitted exterior BCJs with a UHPFRC jacket of thickness 25 mm, observing an increase in the lateral load, ductility, and energy absorption. UHP-HFRC is defined as a material with higher ductility, easy handling, and maintaining structural capacity at large deformation, which requires high fiber contents (4%–11% by volume). The term hybrid refers to the combination of micro-fibers (long smooth, hooked, or twisted fiber) with macro-fibers (short smooth fiber) in the matrix composition [55].

Regarding analytical and numerical models, Bahraq et al. [56] developed the first analytical model to determine the shear strength of BCJs retrofitted with an UHPFRC jacket. In the model, the authors assumed that the contribution of the UHPFRC jacket to the BCJ shear strength could be determined with the formula provided by ACI 352R [57] for normal concrete. The shear strength predictions obtained from the analytical model were compared with the results of finite element models of joints, where the contact between concrete and UHPFRC was implemented using cohesive elements. In the presence of the retrofit intervention, an increase in the load bearing capacity and interface failure mode were observed, as in the experimental tests. However, the simplification of using the formulation of normal concrete for UHPFRC may not lead to reliable results, instead an analytical expression specific for UHPFRC retrofit should be used.

The behavior of RC columns retrofitted with UHPFRC jackets was investigated, through finite element analysis, by Sakr et al. [58], who observed increases in the load capacity with the increase of the UHPFRC jacket thickness. In the model, the interface between the concrete and the jacket was simulated by multi-zero-length connectors, which are two-node connectors placed at the interface, with one node on the concrete and the other on the jacket.

Fayaz et al. [59] performed numerical analyses of BCJs retrofitted with 30 mm thick UHPFRC jacket or UHPFRC jacket confined by CFRP sheets. The models considered perfect bond between concrete and UHPFRC, while the bond between UHPFRC and CFRP was modeled as a tie-bond. The numerical results showed an improvement in shear strength, energy dissipation capacity and structural stiffness, due to the retrofits.

In this research work analytical and numerical models to assess the strength of exterior BCJs retrofitted with UHPFRC jackets are proposed. In particular, an analytical model to calculate the beam flexural strength of RC BCJs retrofitted with UHPFRC jacket, called flexural model from now on is proposed. This model considers the tensile strength contribution of the jacket and it is validated through the comparison with experimental results available in the literature. The flexural model is also used to derive the shear force acting in the joint at beam flexural failure.

Then, an analytical model to calculate the shear strength of exterior BCJs retrofitted with UHPFRC jackets, named herein shear model, is proposed. The model considers the contributions to the joint strength of both the joint core and the UHPFRC jacket, and takes into account the confinement effect produced by the jacket on the joint. The model is validated through the comparison with experimental results available in the literature.

This research work provides also a finite element model of a BCJ retrofitted with UHPFRC jacket. In the FE model, realized using the software ATENA 3D, the concrete-to-steel reinforcement interface interaction is simulated with a bond–slip relationship, while the contact between concrete and UHPFRC is simulated with an interface relationship complying with Mohr–Coulomb criterion [60,61]. To the best of the authors' knowledge, this relationship has not been used to date to reproduce, in BCJs retrofitted with UHPFRC jackets, the interface interaction between the UHPFRC and the concrete of existing elements.

2. Proposed analytical models

2.1. Flexural model

The proposed flexural model is used to calculate the ultimate bending moment of the beam converging to exterior RC BCJs retrofitted with UHPFRC jackets. It is based on the model of Bahraq et al. [56], with respect to which the proposed model assumes a different stress distribution on the cross-section and a different failure mode. Actually, in the proposed model the distribution of the tensile stresses in the jacket is continuous along the height and the failure is due to UHPFRC crushing. Conversely, in [56] the distribution of the tensile stresses in the jacket is not continuous along the jacket's height and the failure is due both to UHPFRC crushing and UHPFRC under tension. The value of the proposed analytical model lies in the possibility of calculating the ultimate bending moment of the retrofitted cross-section without using a software. Actually, the proposed equations can be easily implemented in a spreadsheet. Once this is done, the design of the UHPFRC jacket for the flexural strengthening of a beam can be quickly carried out. The model does not apply to BCJs with pre-deformations before the construction of the strengthening jacket. The model is based on the assumption of plane sections, as the condition of perfect bond between UHPFRC and plain concrete can be achieved by using different techniques of substrate surface preparation, as shown in [34,62–66].

Three possible intervals of the neutral axis depth, x_c, in the beam cross-section are considered, corresponding to Cases 1, 2, and 3. Case 1 occurs when the neutral axis falls entirely in the UHPFRC layer (Fig. 1), of thickness δ_R; Case 2 occurs when the neutral axis is localized between the inner face of the retrofit layer and the centroid of the top reinforcement; finally, Case 3 occurs when the neutral axis is localized below the centroid of the top reinforcement.

The equations proposed in the following are derived for the case in which the flexural failure of the cross-section is due to UHPFRC crushing. Accordingly, it must be checked that, at UHPFRC crushing the strains in the plain concrete and in steel reinforcements do not exceed the ultimate strains. In the following formulation, subscript c refers to the normal concrete, while R to the retrofit material. Fig. 1 shows the distributions of stresses, strains and internal forces on the beam cross-section at joint interface for Case 1. In this case, for convenience of calculation the tensile resultant force is divided in seven components, labeled $T_{R1} - T_{R7}$. The meaning of the symbols used in Fig. 1 is the following: ϵ_{cuR} is the maximum compressive strain in the UHPFRC layer (Eq. 1), $\epsilon_{ut,crack}$ is the strain corresponding to the tensile cracking strength f_{ut} of UHPFRC (Fig. 2); the strains $\epsilon_{ut'}$ and $\epsilon_{ut''}$ and stresses $f_{ut'}$ and $f_{ut''}$ correspond to the horizontal edges of the beam original cross-section (Fig. 2), given by Eqs. (2)–(3) and (8)–(9) in Annex A.1, respectively; ϵ_{ut1} and f_{ut1} are the ultimate tensile strain and stress of UHPFRC; ϵ_{sc} and $\epsilon_{sc'}$ are the strains in the bottom and top longitudinal reinforcements, given by Eqs. (4) and (5), respectively; y is the distance of $\epsilon_{ut,crack}$ (Eq. 7) from the neutral axis; d' is the distance between the extreme compressed concrete fiber of the beam section without jacket and the centroid of the top longitudinal reinforcement; b and h are the width and depth of the beam section without jacket; B and H

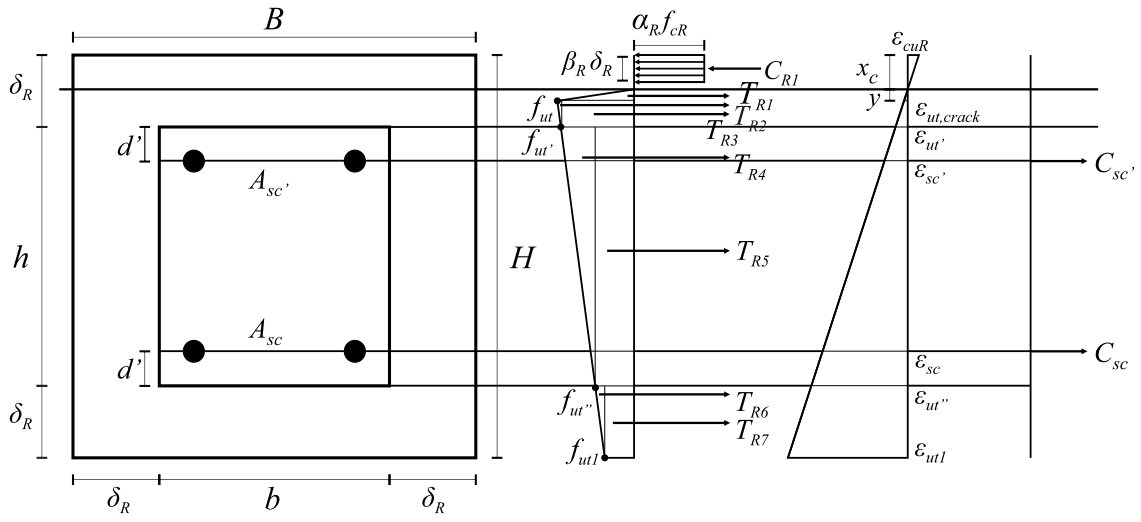

Fig. 1. Distributions of stresses, strains, and forces on the beam cross-section at the interface with the joint retrofitted with UHPFRC jacket — Case 1: $x_c < \delta_R$.

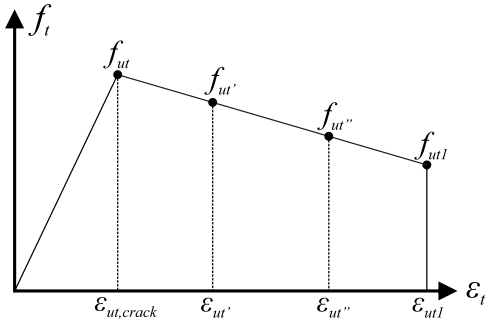

Fig. 2. UHPRFC tensile stress–strain diagram.

are the width and depth of the beam section with jacket; C_{R1} is the compressive force on the UHPFRC layer (Eq. 11). The internal tensile and compressive forces acting on the UHPFRC jacket can be determined by Eqs. (14)–(25); C_{sc} (Eq. (26)) and $C_{sc'}$ (Eq. (27)), ϵ_{sc} and $\epsilon_{sc'}$, A_{sc} and $A_{sc'}$ are the forces, the strains and the areas of the bottom and top longitudinal steel reinforcements, respectively. The yield strength and Young's modulus of steel bars are indicated with symbols f_{sy} and E_s, respectively, in the following. For the tensile behavior of UHPFRC the simplified stress–strain diagram shown in Fig. 2 is adopted, which does not take into account the hardening. This simplification is adopted also in other analytical models present in the literature [30,38,56]. The proposed methodology made this assumption to simplify the analytical equations of the model. This simplification has also been assumed by other authors [30,38,56] The parameters ϵ_{ut} and ϵ_{ut1} correspond to the maximum and ultimate value of tensile strain–stress diagram of UHPFRC, $\epsilon_{ut,crack}$ can be determined from Table A.1 and ϵ_{ut1} is the strain corresponding to f_{ut1}.

The factors α_R and β_R appearing in the equivalent rectangular compressive stress block of UHPFRC are expressed by Eqs. (28) and (29) [67], respectively.

$$\begin{aligned} \alpha_R &\to 0.85 \quad for \quad f_{cR} \le 69 \text{ MPa} \\ \alpha_R &\to 0.85 - 0.0029(f_{cR} - 69) \ge 0.75 \quad for \quad f_{cR} > 69 \text{ MPa} \end{aligned} \tag{28}$$

$$\begin{aligned} \beta_R &\to 0.85 \quad for \quad f_{cR} \le 28 \text{ MPa} \\ \beta_R &\to 0.85 - 0.007252(f_{cR} - 28) \ge 0.65 \quad for \quad f_{cR} > 28 \text{ MPa} \end{aligned} \tag{29}$$

where f_{cR} is the cylindrical compressive strength of UHPFRC. With reference to Fig. 1, the neutral axis depth of the beam cross-section can be determined from the equilibrium of the internal and external axial forces that is:

$$N = 0 = C_{R1} - T_{R1} - T_{R2} - T_{R3} - T_{R4} - T_{R5} - T_{R6} - T_{R7} - C_{sc} - C_{sc'} \tag{30}$$

using the equations in Annex A.1.

Then, the beam flexural capacity can be obtained through the equilibrium of internal and external bending moments calculated with respect to the neutral axis:

$$\begin{aligned} M = C_{R1}\left(\frac{x_c}{2}\right) + T_{R1}\left(\frac{2y}{3}\right) + T_{R2}\left(\frac{\delta_R - x_c - y}{3} + y\right) \\ + T_{R3}\left(\frac{\delta_R - x_c - y}{2} + y\right) + T_{R4}\left(\frac{H - 2\delta_R}{3} + (\delta_R - x_c)\right) \\ + T_{R5}\left(\frac{H - 2\delta_R}{2} + (\delta_R - x_c)\right) + T_{R6}\left(\frac{2\delta_R}{3} + (H - x_c - \delta_R)\right) \\ + T_{R7}\left(\frac{\delta_R}{2} + (H - x_c - \delta_R)\right) + C_{sc}(H - x_c - \delta R - d') + \\ C_{sc'}(\delta R - x_c + d'). \end{aligned} \tag{31}$$

The representations of Cases 2 and 3 are shown in Figs. 3 and 4, respectively, where f_c is the cylindrical compressive strength of normal concrete and C_c is the compressive force in the normal concrete, determined by Eq. 10; C_{R1} and C_{R2} are the compressive forces in the UHPFRC, estimated by Eqs. (12) and (13), respectively; the internal tensile forces of UHPFRC are determined by Eqs. (15)–(23); factors α_c and β_c are determined by Eqs. (32) and (33), respectively, according to the recommendations of ACI 318 [68].

$$\alpha_c \to 0.85 \tag{32}$$

$$\begin{aligned} \beta_c &\to 0.85 \quad for \quad 17 \text{ MPa} < f_c \le 28 \text{ MPa} \\ \beta_c &\to 0.85 - \frac{0.05(f_c - 28)}{7} \quad for \quad 28 \text{ MPa} < f_c < 55 \text{ MPa} \\ \beta_c &\to 0.65 \quad for \quad f_c \le 55 \text{ MPa} \end{aligned} \tag{33}$$

For Case 2 (Fig. 3), the neutral axis depth and the ultimate bending moment of the cross-section are determined by Eqs. (34) and (35), respectively.

$$N = 0 = C_c + C_{R1} + C_{R2} - T_{R1} - T_{R2} - T_{R3} - T_{R4} - T_{R5} - C_{sc} - C_{sc'} \tag{34}$$

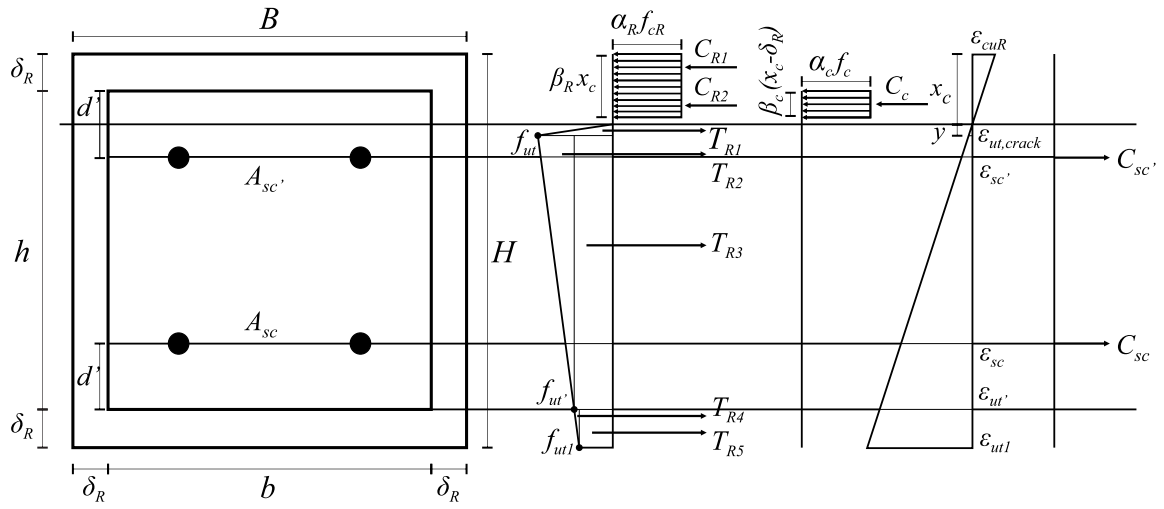

Fig. 3. Distributions of stresses, strains, and forces on the beam cross-section at the interface with the joint retrofitted with UHPFRC jacket — Case 2: $\delta_R < x_c < \delta_R + d'$.

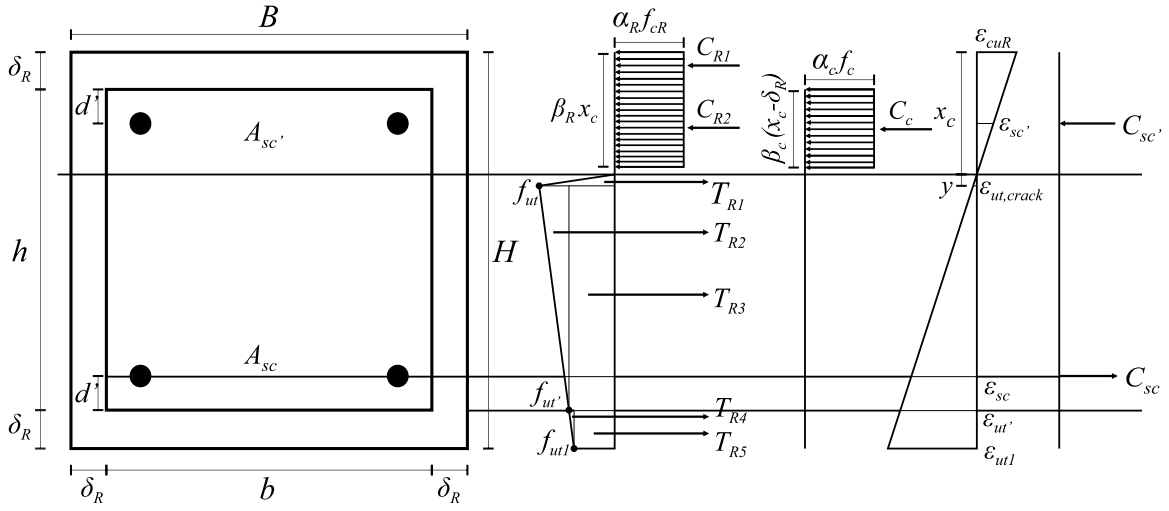

Fig. 4. Distributions of stresses, strains, and forces on the beam cross-section at the interface with the joint retrofitted with UHPFRC jacket — Case 3: $x_c > \delta_R + d'$.

$$
\begin{aligned}
M = {} & C_c\left((x_c-\delta_R)-\frac{\beta_c(x_c-\delta_R)}{2}\right)+C_{R1}\left(x_c-\frac{\delta_c}{2}\right)\\
& +C_{R2}\left((x_c-\delta_R)-\frac{\beta_c x_c-\delta_R}{2}\right)+T_{R1}\left(\frac{2y}{3}\right)\\
& +T_{R2}\left(\frac{H-\delta_R-x_c-y}{3}+y\right)+T_{R3}\left(\frac{h-\delta_R-x_c-y}{2}+y\right)\\
& +T_{R4}\left(\frac{\delta_R}{3}+(H-\delta_R-x_c)\right)\\
& +T_{R5}\left(\frac{\delta_R}{2}+(H-\delta_R-x_c)\right)\\
& +C_{sc}(H-x_c-\delta R-d')+\\
& C_{sc'}(\delta R-x_c+d').
\end{aligned}
\tag{35}
$$

For Case 3 (Fig. 4), the neutral axis depth and the ultimate bending moment of the cross-section are given by Eqs. (36) and (37), respectively. It is observed that, in this case, $\epsilon_{sc'}$ is a compressive strain, differently from that of other cases, and it is expressed by Eq. (33).

$$N = 0 = C_c + C_{R1} + C_{R2} - T_{R1} - T_{R2} - T_{R3} - T_{R4} - T_{R5} - C_{sc} + C_{sc'} \tag{36}$$

$$
\begin{aligned}
M = {} & C_c\left((x_c-\delta_R)-\frac{\beta_c(x_c-\delta_R)}{2}\right)+C_{R1}\left(x_c-\frac{\delta_c}{2}\right)\\
& +C_{R2}\left((x_c-\delta_R)-\frac{\beta_c x_c-\delta_R}{2}\right)+T_{R1}\left(\frac{2y}{3}\right)\\
& +T_{R2}\left(\frac{H-\delta_R-x_c-y}{3}+y\right)+T_{R3}\left(\frac{h-\delta_R-x_c-y}{2}+y\right)\\
& +T_{R4}\left(\frac{\delta_R}{3}+(H-\delta_R-x_c)\right)\\
& +T_{R5}\left(\frac{\delta_R}{2}+(H-\delta_R-x_c)\right)\\
& +C_{sc}(H-x_c-\delta_R-d')+\\
& C_{sc'}(\delta_R-x_c+d').
\end{aligned}
\tag{37}
$$

2.2. Shear model

The proposed shear model is used to estimate the shear strength of exterior RC BCJs retrofitted with UHPFRC jacket. The model assumes that joint failure is due to the attainment of the peak compressive stress in the joint core, taking into account the confinement effect produced by the UHPFRC jacket on the joint core through the confined concrete

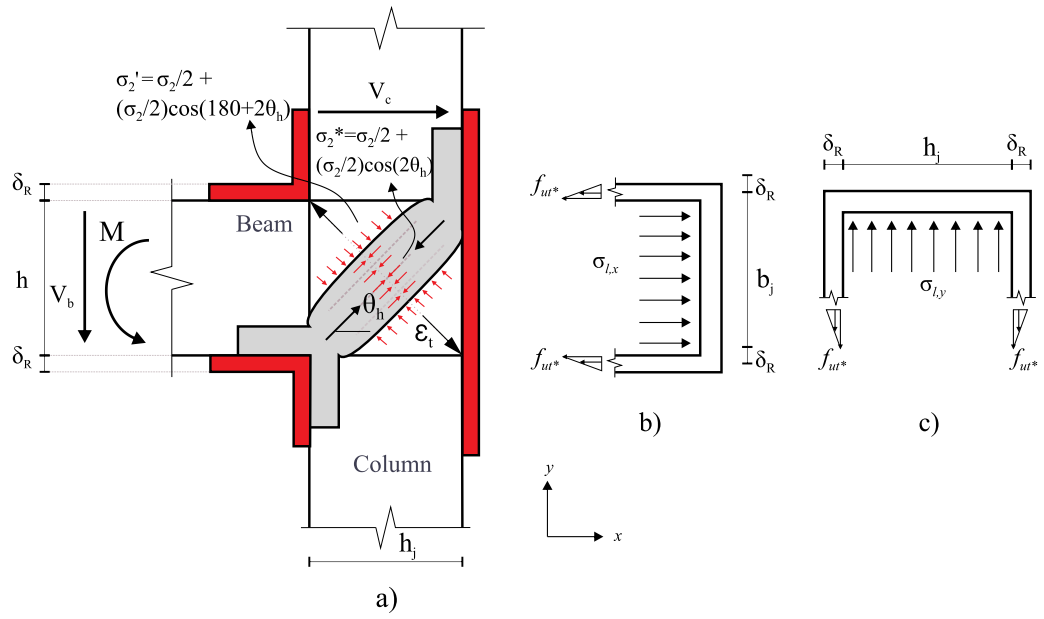

Fig. 5. Confining pressure exerted by UHPFRC jacket on exterior RC beam–column joint: (a) front view, (b) x-direction, (c) y-direction.

strength, f_{cc}. By considering a strut and tie resisting mechanism for the joint, the principal direction of the compression stresses is along the concrete strut, which develops inside the joint core inclined by an angle θ_h with respect to the horizontal plane (Fig. 5.a). Thus, the compressive strain in the confined concrete at the peak stress, $\epsilon_{c2,c*}$, is attained along this direction.

To calculate f_{cc} according to the requirements of the Italian Building Code [69] and Eurocode 2 EN 1992-1-1 [70] an iterative process is used, which is shown in Fig. 6. Since the jacket is in contact with the joint vertical surfaces, to determine the effective mean lateral (horizontal) confining pressure produced by the jacket on the concrete core, σ_2, the horizontal component of the confined concrete strain, ϵ_{th} is considered. The iterative process starts by assuming an initial value of $\epsilon_{c2,c*}$, which can be made equal to the unconfined ultimate compressive strain of normal concrete at peak stress ϵ_{c2} (ϵ_{c2} = 2.0‰ for [69,70]). The transverse strain of the confined concrete strut in the presence of the UHPFRC jacket, ϵ_t, is determined through the use of the Poisson's ratio. For concrete under compression at peak stress, the adopted value of the Poisson's ratio, μ_0, is 0.5, as suggested by Samani and Attard [71]. This value is obtained considering that the axial compressive strain at the instant of zero volumetric strain is approximately equal to the axial compressive strain at which the concrete reaches its peak compressive axial stress.

By assuming a perfect bond at the interface between the joint core and the external jacket, the horizontal strain in the jacket is equal to the normal strain of the confined concrete strut in the horizontal plane, ϵ_{th}. Consequently, the tensile stress in the UHPFRC jacket at the interface with the joint core is obtained from the tensile curve of UHPFRC with the strain value ϵ_{th}.

Since the value of the tensile stress on the external surface is unknown and also the real distribution of the tensile stresses across the jacket is unknown, to take into account that the tensile stress decreases across the jacket thickness, it is assumed that the tensile stress linearly decreases from the inner to the outer surface of the jacket, becoming null on the outer surface. Hence, a triangular distribution of the tensile stresses within the jacket thickness is adopted. The value of the tensile stress in the jacket at the interface with the joint core, f_{ut*}, is calculated from the experimental tensile strain–stress curve.

For the exterior RC BCJ in Fig. 5.a, the lateral pressures exerted by the UHPFRC jacket on the joint core in x and y horizontal directions, $\sigma_{l,x}$ and $\sigma_{l,y}$ in Figs. 5.b and 5.c, respectively, can be estimated by the following equations

$$\sigma_{l,x} = \frac{f_{ut*}\delta_R}{b_j} \tag{38}$$

$$\sigma_{l,y} = \frac{f_{ut*}\delta_R}{h_j} \tag{39}$$

where b_j and h_j are the width and the depth of the joint core, respectively.

Eqs. (38) and (39) are derived assuming that the confinement provided by the UHPFRC jacket and by the beam is uniform on each side of the joint core.

According to the Italian Building Code [69] and Eurocode 2 EN 1992-1-1 [70], the mean lateral confinement pressure, σ_l, can be calculated as the geometrical mean between the two above lateral stresses

$$\sigma_l = \sqrt{\sigma_{l,x}\sigma_{l,y}} \tag{40}$$

The effective mean lateral confining pressure is calculated by

$$\sigma_2 = \alpha\sigma_l; \qquad \alpha = \alpha_n\sigma_s \tag{41}$$

where the coefficients α_n and α_s can be assumed equal to 1, being the UHPFRC jacket continuous and uniform in thickness on the lateral surfaces of the joint.

To calculate the confining pressure orthogonal to the direction of the concrete diagonal strut, σ_2' (Fig. 5.a), the Mohr's circle is used

$$\sigma_2' = \frac{\sigma_2}{2} + \frac{\sigma_2}{2}cos(180 + 2\theta_h) \tag{42}$$

The confined concrete strength can be calculated by [69,70]

$$f_{cc} = f_{ck}\left(1.0 + \frac{5.0\sigma_2}{f_{ck}}\right) \quad \text{for} \quad \sigma_2' \le 0.05 f_{ck} \tag{43}$$

$$f_{cc} = f_{ck}\left(1.125 + \frac{2.5\sigma_2}{f_{ck}}\right) \quad \text{for} \quad \sigma_2' > 0.05 f_{ck} \tag{44}$$

where f_{ck} is the concrete characteristic compressive strength.

The Mohr's circle is also used to determine the compressive stress arising along the axis of the diagonal concrete strut, σ_2^*, due to the confining action of the jacket

$$\sigma_2^* = \frac{\sigma_2}{2} + \frac{\sigma_2}{2}cos(2\theta_h) \tag{45}$$

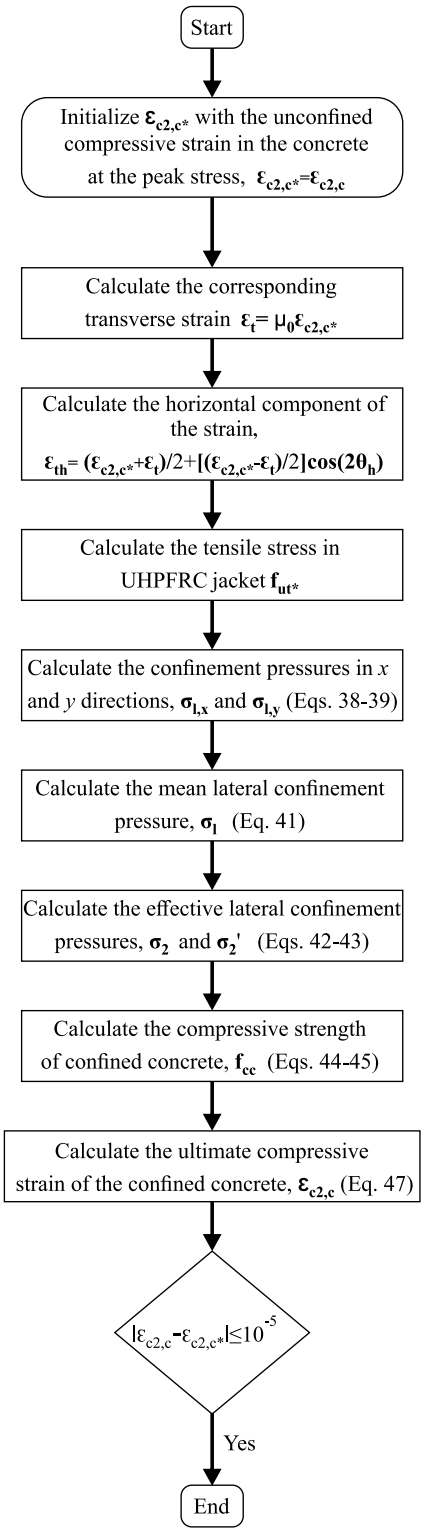

Fig. 6. Iterative process to determine the confined compressive strength of the diagonal strut in exterior BCJs retrofitted with UHPFRC jackets.
Note: f_{ut*} is the tensile stress corresponding to the strain ϵ_{th}, which is obtained from the tensile curve of UHPFRC.

This stress adds to that induced by the lateral load, reducing the maximum stress bearable by the joint. To take account of this, the compressive strength of the strut is calculated by subtracting σ_2^* to the compressive strength of the strut confined concrete.

Finally, the compressive strain in the confined concrete strut at the peak stress, $\epsilon_{c2,c}$ is determined by the following equation [69,70].

$$\epsilon_{c2,c} = \epsilon_{c2} + \frac{f_{cc}}{f_{ck}} \tag{46}$$

The iterative procedure represented in Fig. 6 ends when the absolute value of the difference between $\epsilon_{c2,c}$ and $\epsilon_{c2,c*}$ is $\leq 10^{-5}$.

The shear strength of the retrofitted joint, V_{jh}, is calculated as the sum of the joint core contribution, V_{jhc}, and the UHPFRC jacket. The former is calculated with the formulation of Pauletta et al. [72], considering the confined concrete strength f_{cc} (MPa) in place of f_c and the presence of stress σ_2^*

$$V_{jhc} = 0.71\left[\frac{(\chi f_{cc} - \sigma_2^*)b_j a_c cos(\theta_h)}{\alpha} + 0.79A_h f_{yh} + 0.52\frac{A_v f_{yv}}{tan(\theta_h)}\right] \tag{47}$$

where

$$\chi = \left[0.74\left(\frac{f_{cc}}{105}\right)^3 - 1.28\left(\frac{f_{cc}}{105}\right)^2 + 0.22\left(\frac{f_{cc}}{105} + 0.87\right)\right] \tag{48}$$

$$a_c = \left(0.25 + 0.85\frac{N}{A_g f_{cc}}\right)h_c \tag{49}$$

$$\alpha = \frac{2L_c L_b}{2L_c L_b - (2L_b + h_c)j_{bd}}\left(1 - \frac{l_h\sqrt{f_{cc}}}{\phi_b f_b}\right) \leq 1.0 \tag{50}$$

χ a non-dimensional interpolating function accounting for concrete softening [72], a_c the depth of the compression zone in the column; A_h and f_{yh} the area and the yield strength of joint horizontal reinforcement, respectively; A_v and f_{yv} the area and the yield strength of joint vertical reinforcement, respectively. A_g the gross area of the column section; h_c the height of the column cross-section; j_{bd} the internal moment arm of the beam cross-section, which can be calculated as suggested in [72]; l_h the horizontal projection of the diagonal concrete strut, which is equal to $h_c - a_c$; ϕ_b the mean diameter of beam longitudinal bars in tension; f_b the stress of beam bars in tension (MPa).

In this condition, the acting shear force V_{jh}^A distributes between the joint core and the UHPFRC jacket in relation to their shear stiffness, that is

$$V_{jhc}^A = V_{jh}^A\left(\frac{G_c A_c}{G_c A_c + G_R A_R}\right) \tag{51}$$

$$V_{jhR}^A = V_{jh}^A\left(\frac{G_R A_R}{G_c A_c + G_R A_R}\right) \tag{52}$$

with G_c and G_R the shear modulus of the normal concrete and of UHPFRC, respectively, A_c the joint core horizontal area and A_R the UHPFRC jacket horizontal area at mid-height of the joint, as shown in Fig. 7.b. The shear moduli of normal concrete, G_c, and UHPFRC, G_R, can be calculated by means of Eq. (53), using the values of the Young's modulus and Poisson's ratio of the materials. Concrete and UHPFRC Young's moduli, E_c and E_R, respectively, can be obtained from experimental results. Alternatively, E_c can be calculated according to ACI 318 recommendations [68] (Eq. (54)), while E_R through the formula developed by Guo et al. [73], expressed by Eq. (55) (f_c and f_{cR} in MPa). With regard to the Poisson's ratios, ν, the value of 0.2 is adopted both for normal concrete and UHPFRC, as recommended by ACI 318 [68], French Standard [49] and in the studies of Russell et al. [74].

$$G = \frac{E}{2(1+\nu)} \tag{53}$$

$$E_c = 4700\sqrt{f_c} \tag{54}$$

$$E_R = 3837\sqrt{f_{cR}} \tag{55}$$

The contribution of the UHPFRC jacket to shear strength is determined in function of the contribution provided by the concrete strut, assuming that both the jacket and the concrete core are in the elastic field.

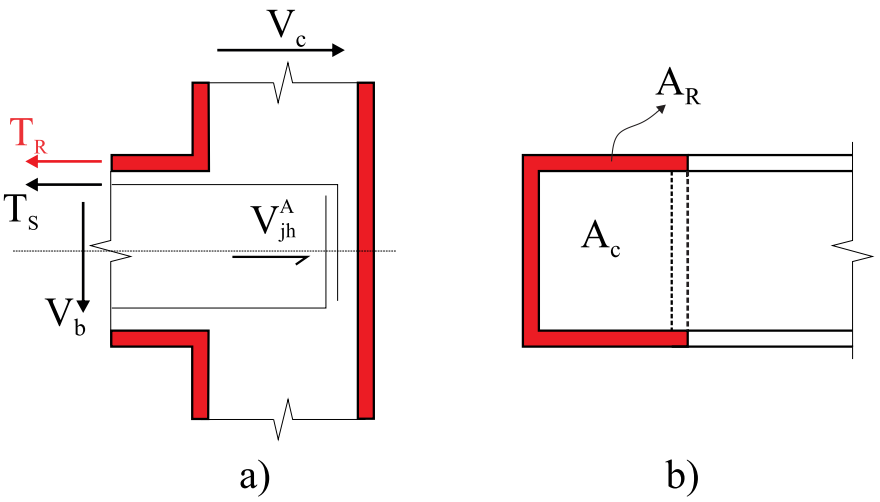

Fig. 7. Scheme of the retrofitted joint: (a) vertical section, (b) horizontal section at mid-height.

Assuming that the jacket percentage contribution to joint shear strength is that considered in Eqs. (51) and (52), the joint shear strength is calculated as follows

$$V_{jh} = V_{jhc} + V_{jhc}\frac{G_R A_R}{G_c A_c} \tag{56}$$

In order to avoid joint shear failure, the joint shear strength must be greater than the shear force on the joint acting at beam flexural failure. In this condition, the acting shear force, V_{jh}^{A}, can be calculated from the equilibrium of the top half part of the joint, as shown in Fig. 7a. Considering that a negative bending moment acts on the beam cross-section, V_{jh}^{A} is given by the sum of the tensile force on the retrofit material, T_R, the tensile force on the top reinforcement, T_s, and the shear force on the column, V_c, as follows

$$V_{jh}^{A} = T_R + T_s - V_c \tag{57}$$

where

$$T_s = A_s f_y \tag{58}$$

$$V_c = \frac{L_b V_b}{L_c} \tag{59}$$

with A_s the area of the top steel reinforcement; ϵ_s the tensile strain in the top steel reinforcement (at the ultimate bending moment); V_b the shear acting on the beam; L_b and L_c the lengths of the beam and the column, respectively (see Fig. 8).

To provide the joint with adequate ductility, the UHPFRC jacket should be designed to promote the flexural failure of the beam. To this aim, the value of V_b in Eq. (59) can be determined considering the attaining of the ultimate bending moment in the beam, calculated as described in Section 2.1.

The total shear force acting in the joint can also be expressed as the sum of the joint shear forces acting in the joint core, V_{jhc}^{A}, and in the UHPFRC jacket V_{jhR}^{A}, i.e.

$$V_{jh}^{A} = V_{jhc}^{A} + V_{jhR}^{A} \tag{60}$$

3. Numerical model

In order to provide a numerical model of BCJs retrofitted with UHPFRC jackets, a numerical simulation of the beam–column joints studied by Beschi et al. [26] is performed. As Beschi et al. [26] tested two identical joints, one without retrofit and the other retrofitted with a HPFRC jacket, specimens CJ2 and RCJ2, respectively, two models corresponding to these specimens are implemented herein. The

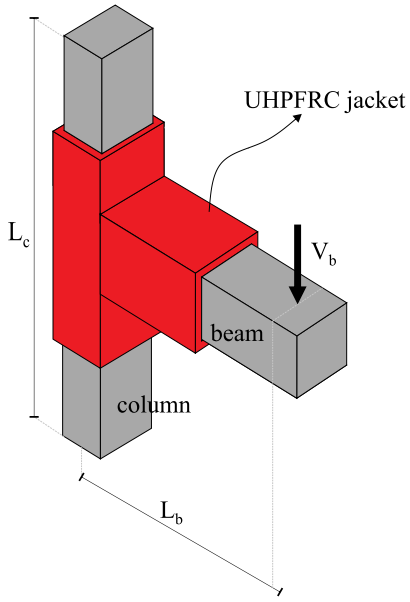

Fig. 8. Scheme of exterior beam–column joint retrofitted with UHPFRC.

pre-processing and geometry of the joints are developed using the GID program (version 16.0.1), while the post-processing is carried out by ATENA 3D software (version 5.9.0) using the Finite Element Method [60]. Both the BCJs' numerical models are subjected to the same cyclic displacement history, applied to the column during the tests. Details regarding the properties of the tested specimens and the performed tests are reported below.

3.1. Experimental test

The main geometric and mechanical characteristics of the tests carried out by Beschi et al. [26] are presented in the following.

3.1.1. Geometry

The dimensions of the beam and column cross-sections of the tested joints were 300 × 500 mm^2 and 300 × 300 mm^2, respectively. The total height of the column, L_c, and the length of the beam, L_b, corresponding to the contra-flexure points placed in the beam mid-span and column mid-height of a real building frame, were 3000 mm and 2100 mm, respectively, as shown in Fig. 9.

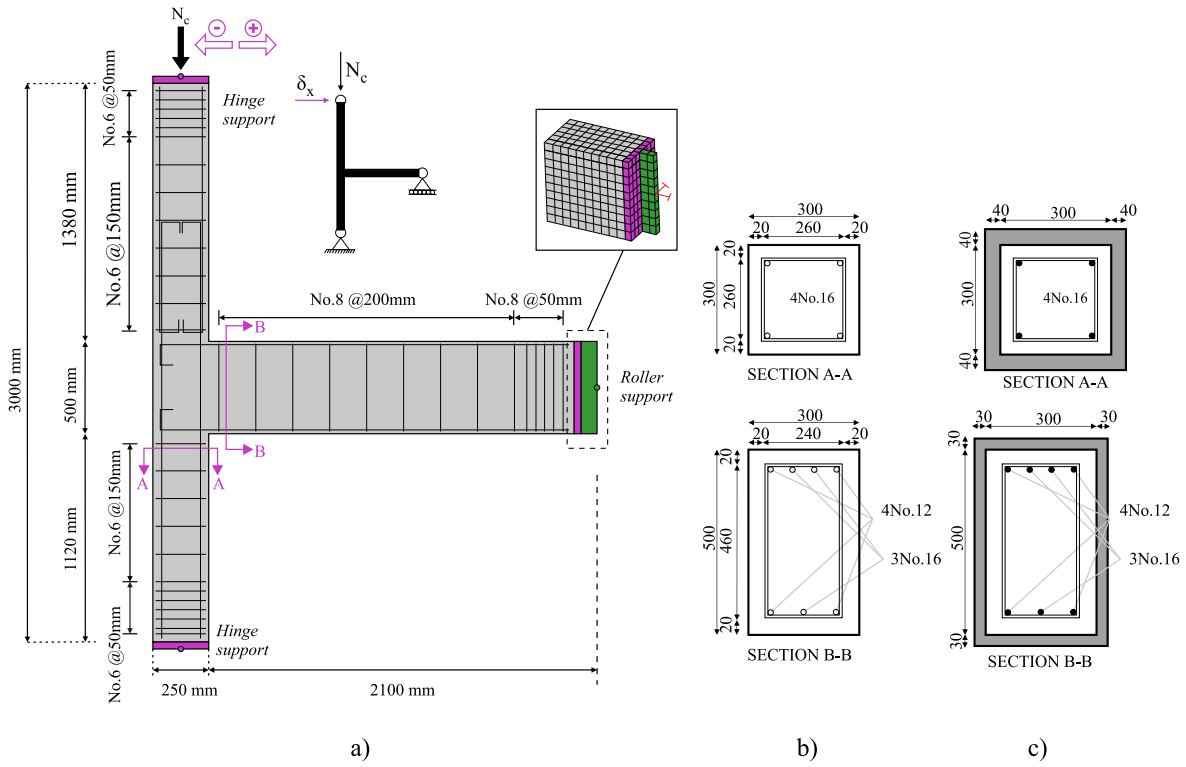

Fig. 9. Geometrical details of: (a) beam–column joint, (b) sections of sub-assemblage CJ2, and (c) sections of sub-assemblage RCJ2 [26].

3.1.2. Materials' properties and reinforcement details

The normal concrete of CJ2 and RCJ2 specimens had a cylinder compressive strength of 38.7 MPa and 27 MPa, respectively, and a Young's modulus of 29238 MPa and 24421 MPa, respectively. The HPFRC material had a compression strength of 111 MPa, a Young's modulus of 36000 MPa, and a tensile strength of 6.6 MPa. The thickness of the HPFRC jacket was 30 mm in the beam and 40 mm in the column.

The longitudinal reinforcement of the beam was constituted by 4 smooth steel bars of diameter 12 mm (two localized at the bottom and two at the top) and 3 bars of diameter 16 mm with end-hooks in the region of the joint core, as shown in Fig. 9. The longitudinal reinforcement of the column was composed of 4 steel bars of diameter 12 mm with a lap-splice in the superior column. Regarding the transverse reinforcement, the beam had stirrups of diameter 8 mm, spaced 200 mm (50 mm in the beam end), and the column had stirrups of diameter 6 mm, spaced 150 mm (50 mm in the column ends). No transverse reinforcement was placed in the joint core. The steels of bars with diameter 12 mm and 16 mm presented yield strengths of 365 MPa and 445 MPa, ultimate strengths of 558 MPa and 546 MPa, and ultimate strains of 15.9% and 13.7%, respectively. Stirrups with 6 mm and 8 mm diameter had yield strengths of 493 MPa and 337 MPa, ultimate strengths of 556 MPa and 440 MPa, and ultimate strains of 16.1% and 21%, respectively. The steel Young's modulus was assumed equal to 200000 MPa.

3.1.3. Loading and boundary conditions

In the experimental test, two hydraulic jacks were used to apply the vertical load of 210 kN at the column top to simulate the gravity load. The horizontal cyclic displacement was applied through an electromechanical jack fixed to a strong wall and to the column top. The load is considered positive in the left-to-right direction. The beam–column joint presented free rotation at the top and at the base of the column (hinge supports). The beam end was subjected to restriction only in the vertical direction through a roller support. These boundary conditions were applied to both specimens.

3.2. Materials' constitutive models

3.2.1. Concrete

ATENA 3D allows the simulation of the materials' nonlinear behavior, such as concrete and steel. In the BCJs' models presented herein, concrete is implemented using the *CC3DNonLinearCementitious2* material model, which is characterized by a fracture-plastic constitutive relationship that considers the material's cracking behavior and plasticity. The concrete compression stress–strain curve is composed of a first hardening branch (Fig. 10a) followed by a softening branch (Fig. 10b), separated by the point where the compressive stress reaches the peak value, f_c' [60]. In the post-peak branch, the strains are converted in crack width, w, where w_d is the plastic displacement, and L_{co} is the crack band size, calculated as the projection size into the direction of minimum principal stresses, following the model proposed by Van Mier [75]. To simulate concrete plastic compressive behavior, ATENA adopts the triaxial failure surface developed by Menetrey and William [76]

$$F(\xi,\rho,\theta)=\left[\sqrt{1.5}\frac{\rho}{f_c'}\right]^2+m\left[\frac{\rho}{\sqrt{6}f_c'}r(\theta,e)+\frac{\xi}{\sqrt{3}f_c'}\right]-c=0 \tag{61}$$

where θ is the deviatoric polar angle, ξ and ρ are the hydrostatic and deviatoric stress invariants, respectively; f_c' is the axial compressive strength; c and m are the concrete friction and cohesion parameters; r is an elliptic function, depending on the parameter e, which defines the surface roundness. The failure surface has sharp corners for e=0.5 and it is fully circular for e=1.0.

Concrete tensile behavior (Fig. 10c) is governed by Hordijk's softening function [77], where G_f is the fracture energy, σ is the normal tensile stress, w_c is the crack opening when the energy is dissipated, given by Eq. (62), and L_t is the crack band size determined from the element projection in the direction orthogonal to the crack.

$$w_c=5.14\frac{G_f}{f_t} \tag{62}$$

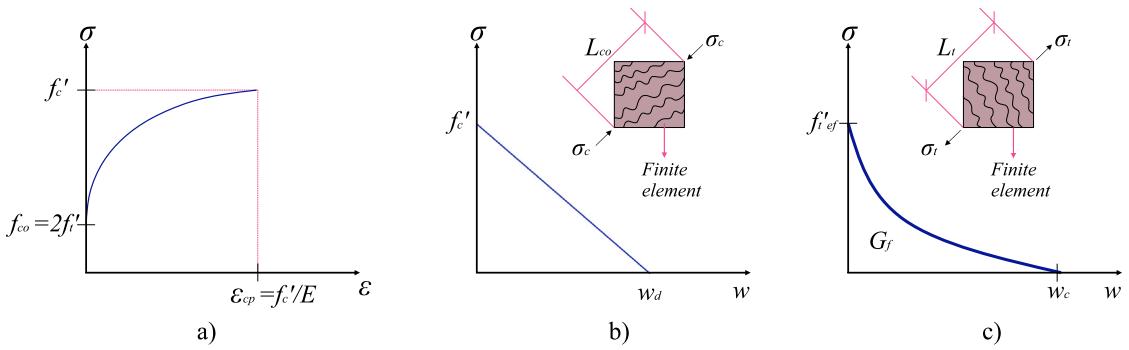

Fig. 10. Compression models [60] of (a) hardening and (b) softening branches; and (c) tensile softening model of Hordijk [77].

Table 1
Concrete properties used in the numerical models of BCJs.

Parameter	Specimen CJ2	Specimen RCJ2
Compressive strength (f_c) [26]	38.7 MPa	27 MPa
Young's modulus (E_c) [68]	$4700\sqrt{f_c}$	$4700\sqrt{f_c}$
Poisson's ratio [68]	0.2	0.2
Tensile strength (f_t) [78]	$0.23(f_c)^{(2/3)}$	$0.23(f_c)^{(2/3)}$
Fracture energy (G_f) [79]	$73f_c^{0.18}$	$73f_c^{0.18}$
Tension stiffening	0.05	0.05
Aggregate size	20 mm	20 mm
Shear factor (S_f)	60	60
Plastic strain at compressive strength (ϵ_c^p) [60]	0.00115	0.00137
Strength at the onset of nonlinear behavior - (f_{co}) [60]	5.6 MPa	4.50 MPa
Reduction factor of compression [60]	0.8	0.8
Eccentricity (e) [60]	0.5	0.5
Flow plastic (β) [60]	0.5	0.5
Crack orientation [60]	Fixed	Fixed

Table 2
Steel properties used in the numerical models of BCJs.

Parameter	Bars with ϕ=6 mm/8 mm	Bars with ϕ=12 mm/16 mm
Young's modulus (E_s)	200000 MPa	200000 MPa
Yield strength (f_y) [26]	493 MPa/337 MPa	365 MPa/445 MPa
Ultimate strength (f_u) [26]	556 MPa/440 MPa	558 MPa/546 MPa
Ultimate strain [26]	0.161/0.21	0.159/ 0.137
Menegotto–Pinto [80]	R=20, C1=0.925, C2=0.15 [60]	R=20, C1=0.925, C2=0.15

The values of the parameters used for modeling the normal concrete are expressed in Table 1.

The incremental formulation of CC3DNonLinearCementitious2 material allows to describe both the monotonic and the cyclic behavior of concrete.

3.2.2. Reinforcement

For the transverse and longitudinal reinforcements, the stress–strain relationship provided by the *CCCyclingReinforcement* material model is used.

The cyclic behavior of steel reinforcement was reproduced through Menegotto–Pinto model [80], which takes into account Bauschinger's effect. The Menegotto–Pinto model is governed by 3 parameters: the curvature R, and the experimental coefficients c_1 and c_2 [60]. The values of the parameters used for modeling the steel reinforcements are expressed in Table 2.

3.2.3. HPFRC

To model the HPFRC material, the *CC3DNonLinearCementitious2user* model is used, which allows to specify defined relationships for tensile and compression behaviors, combining the fracture and the plasticity models of the material [60]. In the experimental campaign of Beschi et al. [26] also two direct tensile tests, known as 'dog-bone' tests, were performed on HPFRC. These tests provided maximum tensile strength values of 7.5 MPa and 5.7 MPa, with an average tensile strength of 6.6 MPa and a strain-hardening up to 0.15% strain [26].

To check the reliability of the simplified stress–strain diagram used to describe the HPFRC tensile behavior, the "dog-bone" specimen also is modeled by ATENA. It was based on the experimental results, which was considered linear up to the stress value of 6.6 MPa. The modeling of the HPFRC material was made according to the numerical model developed in [38], where the UHPFRC tensile behavior is modeled by a linear elastic branch up to the microcracking onset, followed by a linear branch in the phase of strain hardening, characterized by multiple microcracking, and then by a descending bi-linear branch, representing the softening phase after the formation of the first macrocrack.

In the *CC3DNonLinearCementitious2user* model the tensile behavior is described by the fracturing strain, $\epsilon_1^{f'}$, which is calculated as shown by Eq. (63), where: ϵ_1^f is the fracturing strain calculated from the strain tensor at the finite element integration points, ϵ_{loc}^f is the strain after which strain localization can be expected, L_t is the crack band size and L_{ch}^t is the characteristic length. In the model, L_{ch}^t was taken equal to 80 mm.

$$\epsilon_1^{f'} = \epsilon_1^f \quad for \quad \epsilon_1^f < \epsilon_{loc}^f$$
$$\epsilon_1^{f'} = \epsilon_{loc}^f + (\epsilon_1^f - \epsilon_{loc}^f)\frac{L_t}{L_{ch}^t} \quad for \quad \epsilon_1^f > \epsilon_{loc}^f \tag{63}$$

The "dog-bone" dimensions of 0 × 330 × 15 mm^3 and a mesh size of 50 × 15 × 15 mm^3 are used. Regarding boundary conditions, the displacement at the bottom edge of the "dog-bone" model is restrained, while a vertical displacement is applied to the top edge, similarly to the

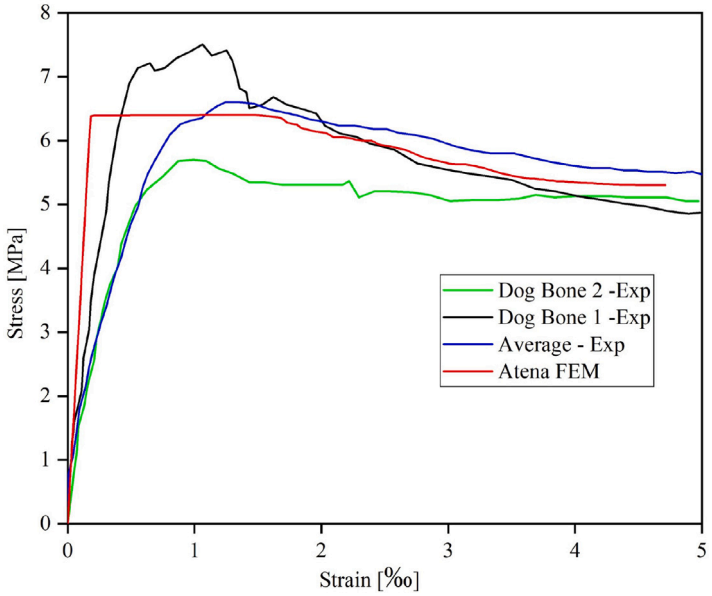

Fig. 11. Comparison between experimental and numerical functions of HPFRC tensile behavior.

laboratory test. The experimental stress–strain diagrams of the tested specimens are reported in Fig. 11, together with the results obtained by the numerical model. The average behavior of the two tested specimens, represented by the blue curve, is used for the comparison with the results obtained from ATENA model (in red). From Fig. 11, it can be observed that the numerical model predicts quite well the peak load, maintaining on the safe side, and very good softening behavior, even if the numerical model shows to be a little stiffer than the "dog-bone" specimens. Hence, the function used in ATENA to implement the HPFRC material can be considered satisfactorily reliable.

The incremental formulation of *CC3DNonLinearCementitious2user* material allows to describe both the monotonic and the cyclic behavior of UHPFRC.

3.2.4. Concrete–steel interface

To simulate the bond behavior between the smooth longitudinal steel bars and concrete in the joint models, the concrete–steel interface was modeled through the *Memory Bond Material* model (Table 2), following the recommendations of [60] to capture the structural response during cyclic loads. After the bond stress sign changes, instead of following the same envelope as during loading, the maximum bond stress is determined by the parameter τ_1, which can vary between the residual stress (τ_{res}), i.e. the last stress value of the bond strength-slip function, and the maximum bond stress (τ_{max}), as shown in Fig. 12, where s is the slip and τ is the bond strength [60]. A good bond between concrete and steel, and a maximum bond strength τ_{max} of 1.6 MPa, determined according to the design criteria of CEB-FIP Model Code [79] was adopted. For the stirrups perfect bond with the concrete was assumed.

3.2.5. Concrete-HPFRC interface

In the finite element model of specimen RCJ2, the contact between concrete and HPFRC was simulated through the *Interface* material model, which is formulated to reproduce both monotonic and cyclic load conditions [81,82]. This model is based on the Mohr–Coulomb criterion with a tension cut-off. After stress reaches this condition, the surface collapses to a residual surface, representing a dry condition between the materials [60]. The interface is governed by the initial normal and tangential stiffnesses, K_{nn} and K_{tt}, respectively, the minimal normal and tangential stiffnesses, K_{nn}^{min} and K_{tt}^{min}, respectively, the friction coefficient, μ, the tensile strength, $f_{t,int}$, and the cohesion coefficient, c. The minimum stiffness values K_{nn} and K_{tt} are used only for numerical purposes after the element failure, to preserve the positive definiteness of the global system of equations. These stiffness values should be chosen approximately 0.001 times the initial stiffness values [60]. In cases where no experimental information on the interface material is available, μ can be assumed between 0.3 and 0.5 (except for oiled surface), $f_{t,int}$ between 0.25 and 0.5 times the tensile strength of the material with the lowest strength and c between 1 and 2 times the interface's tensile strength [60]. The parameters used in the numerical model presented herein, are reported in Table 3.

Table 3
Properties of the interface material used in the numerical model of specimen RCJ2.

Parameter	3D interface
Normal stiffness (K_{nn})	1.4×10^6 MN/m^3
Tangential stiffness (K_{tt})	1.4×10^6 MN/m^3
Minimal Normal stiffness (K_{nn}^{min})	1.4×10^3 MN/m^3
Minimal Tangential stiffness (K_{tt}^{min})	1.4×10^3 MN/m^3
Friction coefficient (μ)	0.5
Tensile strength ($f_{t,int}$)	3.0 MPa
Cohesion coefficient (c)	1.0 MPa

3.3. Model setup

The beam–column joints without and with HPFRC jacket, CJ2 and RCJ2 respectively, are simulated through tridimensional models (Fig. 13). These models include concrete elements (beams and columns), steel bars and stirrups, HPFRC jacket, and steel plates representing the joint restraints.

The concrete beam and column are modeled using hexahedral finite elements with eight nodes and eight integration points. The steel longitudinal bars and stirrups are modeled using truss finite elements with two nodes and two integration points. The steel plates are modeled through the *CC3DElastIsotropic* material model, using hexahedral finite elements with four nodes and four integration points. The beam–column joints have a mesh of 50 × 50 × 50 mm^3 composed of 4722 elements and 24805 nodes for CJ2, and 16624 elements and 20016 nodes for RCJ2. The loading history of both specimens is simulated through load intervals, where the first interval is used to apply the axial load at the top of the column. In the other subsequent intervals, displacement cycles with increasing values of the maximum displacement are applied. The first displacement step amplitude is ±15 mm.

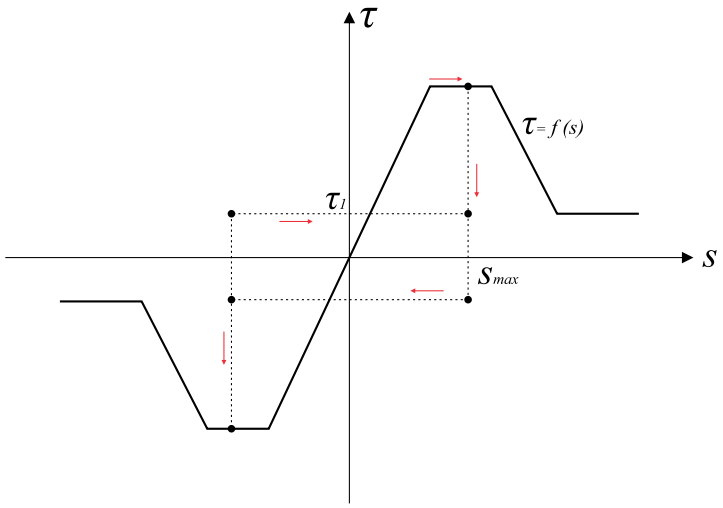

Fig. 12. Bond stress–slip relationship of *Memory Bond* material [60].

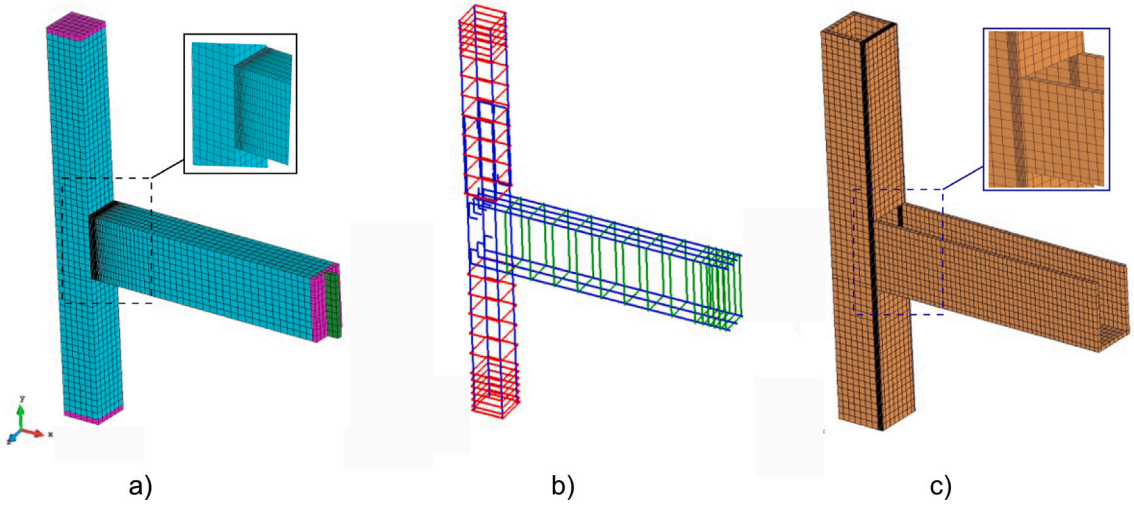

Fig. 13. Discretization mesh of (a) concrete and restraints of CJ2, (b) reinforcement of CJ2, and (c) HPFRC of RCJ2.

For specimen CJ2 the analysis was carried out up to the maximum displacement reached in the experimental test, equal to 75 mm. Conversely, for specimen RCJ2 the numerical analysis was carried out up to 31 mm displacement, in correspondence of which the softening of the specimen already started. Since the aim of the analyses is the determining the maximum load bearable by the beam–column joint, the analyses were stopped at a displacement value a little greater than the displacement, obtained by the test, at the peak load of the first cycle immediately after the cycle with the maximum load. Overall specimen CJ2 is subjected to 13 displacement steps, while specimen RCJ2 is subjected to 15 steps.

The Modified Newton–Raphson iterative solver is used, with a maximum number of iterations equal to 300. For the convergence, the maximum allowed errors are 1% for relative error in displacement and residual force, and relative error in residual force components, and 0.1% for relative error in energy.

4. Models validation

4.1. Flexural model

The analytical flexural model proposed in this work is validated by comparison with experimental test results available in the literature. The research works providing all the required data for applying the proposed model, and in particular the experimental tensile stress–strain diagram of the retrofitting material, concern three RC columns (R-30, R-25, and Test 1) [42,58] and four RC beam–column joints (R-SED, RCJ2, TS1, and RS-UHPFRC-C) [26–29]. All the joint specimens underwent flexural failure.

Table 4 summarizes the specimens' properties necessary for the application of the flexural model formulations (see Section 2.1). Due to the insufficient experimental information about the UHPFRC tensile behavior of specimens tested by Sharma and Bansal [28] and Saharan et al. [29] (specimens R-SD and RS-UHPFRC-C, respectively), for these specimens it is assumed the same UHPFRC tensile strain–stress curve obtained by Khan et al. [27]. The tensile strength f_{ut} used was similar to the formula of Graybeal [83] (Eq. (64)) and provisions given by the French Standard [49] (f_{cR} in MPa).

$$f_{ut} = \frac{6.7\sqrt{f_{cR}}}{\sqrt{145}} \tag{64}$$

The ultimate bending moment values obtained from the analytical flexural model, M_{ana}, are reported in Table 5, together with the corresponding experimental values, M_{exp}. Due to the presence of axial force in the column specimens, the ultimate bending moment of the specimens R-30, R-25 and Test 1 has been calculated with respect to the axis passing through the geometric centroid of the column cross-section. From this table it can be seen that all the analytical values of

Table 4
Specimens properties used for the flexural model validation.

Specimen	δ_R [mm]	B [mm]	H [mm]	L_b [mm]	L_c [mm]	f_c [MPa]	f_{cR} [MPa]	f_{sy} [MPa]	A_{sc} [mm^2]	$A_{sc'}$ [mm^2]	f_{ut} [MPa]	f_{ut1} [MPa]	$\epsilon_{ut,crack}$	ϵ_{ut}
R-30 [58]	30	360	360	–	–	18	150	360	402.1	402.1	4.9	3.0	0.00012	0.009
R-25 [58]	25	350	350	–	–	18	150	360	402.1	402.1	4.9	3.0	0.00012	0.009
Test 1 [42]	60	280	280	–	–	13	107	450	226.2	226.2	3.8	0.6	0.000103	0.10
R-SED [28]	25	125	225	950	1000	25.6	107	415	235.6	157.1	7.5	4.4	0.00014	0.011
RCJ2 [26]	30	360	530	2100	3000	27	111	365	427.3	628.3	6.6	6	0.001	0.005
TS1 [27]	30	260	310	925	1025	30	145	605	1256.3	1256.3	7.5	4.4	0.00014	0.011
RS-UHPFRC-C [29]	25	125	225	950	1000	26.3	122	415	235.6	157.1	7.5	4.4	0.00014	0.011

Table 5
Analytical and experimental moments and shear actions.

Specimen	x_c [mm]	M_{ana} [kN m]	M_{exp} [kN m]	Error - M [%]
R-30 [58]	9.4	72.1	74.2	2.8
R-25 [58]	8.8	65.7	67.7	3.0
Test 1 [42]	11.8	38.2	34.9	9.5
R-SED [28]	18.6	27.9	25.3	10.3
RCJ2 [26]	40.6	149.9	148.5	0.9
TS1 [27]	67.6	188.7	193.3	2.4
RS-UHPFRC-C [29]	18.9	27.9	32.9	15.2

the bending moment are close to the experimental ones. The maximum moment differences, 10.3% and 15.2%, occur for specimens R-SED [28] and RS-UHPFRC-C [29], respectively, for which the tensile strain–stress behavior of the UHPFRC was unknown and it is calculated herein through Eq. (64). In all the other cases the absolute percentage error is lower than 9%.

It can be concluded that when all the required properties are known, the proposed flexural model guarantees good reliability in the prediction of the ultimate bending moment of RC beams converging to beam–column joints strengthened by UHPFRC jackets. When this moment acts on the beam cross-section at the joint interface, the corresponding acting shear can be easily calculated form the equilibrium of the beam as M_{ana}/L_b.

4.2. Shear model

The analytical shear model proposed in this work is used to calculate the joint shear strength of specimens available in the literature tested under cyclic loads. The research works providing all the required data for applying the proposed model concern three exterior beam–column joints subjected to cyclic load (R-SED, RCJ2, and RS-UHPFRC-C) [26,28,29], respectively.

Table 6 summarizes the specimens' properties necessary for applying the shear model formulation (see Section 2.2). The same table shows also the analytically determined values of the shear force transferred by the beam to the joint, V_{jh}^A (Eq. (57)), and the rates of the shear force distributed to the joint core and the UHPFRC jacket, V_{jhc}^A and V_{jhR}^A respectively. Also the analytical values of the shear in the column, V_c, calculated by the Eq. (59) are provided.

The effective mean lateral confining pressure, σ_2 (Eq. (41)), and the confined concrete compressive strength, f_{cc} (Eqs. (43)–(44)), are also shown in Table 6. By comparing the values of f_{cc} reported in Table 6 with the values of f_c reported in Table 4, an increase of at least 9.4% in the compressive strength is observed. The concrete contribution to the joint shear strength, V_{jhc}, and the total shear force, V_{jh}, also shown in Table 6, are determined through Eqs. (47) and (56), respectively. From these values and considering Eq. (56), it can be concluded that, in 2 out of 3 cases, the main contribution to the joint shear force is given by the second member of the equation, $V_{jhc}(G_R A_R/G_c A_c)$, which is due to the UHPFRC jacket. In fact, the percentage contributions of the jacket to joint shear strength are 65.6%, 28.6%, and 67.2% for specimens R-SED, RCJ2, and RS-UHPFRC-C, respectively.

By comparing the values of the acting shear force, V_{jh}^A, and the shear strength, V_{jh}, reported in Table 6, it can be observed that, for all the strengthened specimens, the latter is higher than the former, with percentage differences of 33.3%, 27.1% and 49.9%, for specimens R-SED, RCJ2 and RS-UHPFRC-C, respectively. On the basis of this comparison, it can be said that no specimen undergoes joint shear failure, correspondently to the experimental evidences. In the proposed shear model the shear strength contribution of the jacket is quantified, in Eq. (56), as the product between the shear strength of the joint core and the ratio between the shear stiffness of the jacket and that of the joint core. When the joint core is subjected to shear forces, after the occurring of the first plastic damage, the shear force in the concrete diagonal strut continues to increase, until the peak shear stress is reached, and, then, decreases. Due to the plastic damage caused by cracking, the shear stiffness of the joint core reduces. According to Eq. (56), if the shear modulus of the joint core, G_c, reduces, the second term of the equation, which represents the jacket contribution to joint shear strength, increases, until the peak load is reached. Consequently, considering the elastic shear moduli in Eq. (56) leads to underestimating the jacket contribution to the joint shear strength.

For this reason, the fact that the predicted shear strengths of specimens in Table 6 are always higher than the shear actions appears correct. Being the shear strength of the BCJs unknown, since the specimens underwent beam flexural failure, this is the only possible comparison which can be made. In fact, it appears improbable that BCJs reinforced by UHPFRC jackets fail due to shear, since the jacket is used to increase the shear strength of the joints so as to promote the flexural failure of the beam, preventing joint shear failure, which is an unwanted brittle mechanism. Moreover, the accuracy of the proposed model in predicting each of the two contributions to joint shear strength, V_{jhc} and V_{jh}^R, provided by the joint core and the jacket, respectively, has been checked. In particular, it has been observed that V_{jhc} and V_{jh}^R are always greater than the maximum shear force acting, respectively, in the core and in the jacket, V_{jhc}^A and V_{jhR}^A, respectively. All these results allow to conclude that the model is able to predict that the joint, both in the overall and in its components is subjected to actions lower than those producing shear failure. Moreover, they highlight the efficacy of UHPFRC as retrofitting material to avoid undesirable shear failure in non-seismic exterior beam–column joints subject to cyclic load.

4.3. Numerical model

The comparison between the finite element models and the experimental results is shown in Figs. 14 and 15, for specimens CJ2 and RCJ2, respectively.

By considering Fig. 14, the following observations can be made:

- The numerical simulations of the RC BCJ without retrofit, CJ2, obtained applying one and three cycles for each displacement step show that the first cycles of the load–displacement curve obtained with one cycle and three cycles are very similar up to the maximum load. Both the numerical curves are a little stiffer than the experimental curve representing the first cycle for each displacement step.

Table 6
Acting shear forces and shear strengths of BCJ specimens.

Specimen	E_c [MPa]	E_R [MPa]	G_c [MPa]	G_R [MPa]	T_R [kN]	V_c [kN]	V_{jhc}^A [kN]	V_{jhR}^A [kN]	V_{jh}^A [kN]	σ_2 [MPa]	f_{cc} [MPa]	V_{jhc} [kN]	V_{jh}^R [kN]	V_{jh} [kN]
R-SED [28]	23 780	39 614	9908	16 505	38.3	27.9	38.9	74.1	113.1	1.57	29.53	51.9	98.9	150.8
RCJ2 [26]	24 421	36 000	10 175	15 000	158.6	49.99	194.4	77.9	272.4	0.65	29.55	247.1	99.1	346.2
RS- [29]-UHPFRC-C	23 654	42 381	9856	17 658	38.3	32.8	35.5	72.7	108.2	1.57	30.26	53.2	108.9	162.1

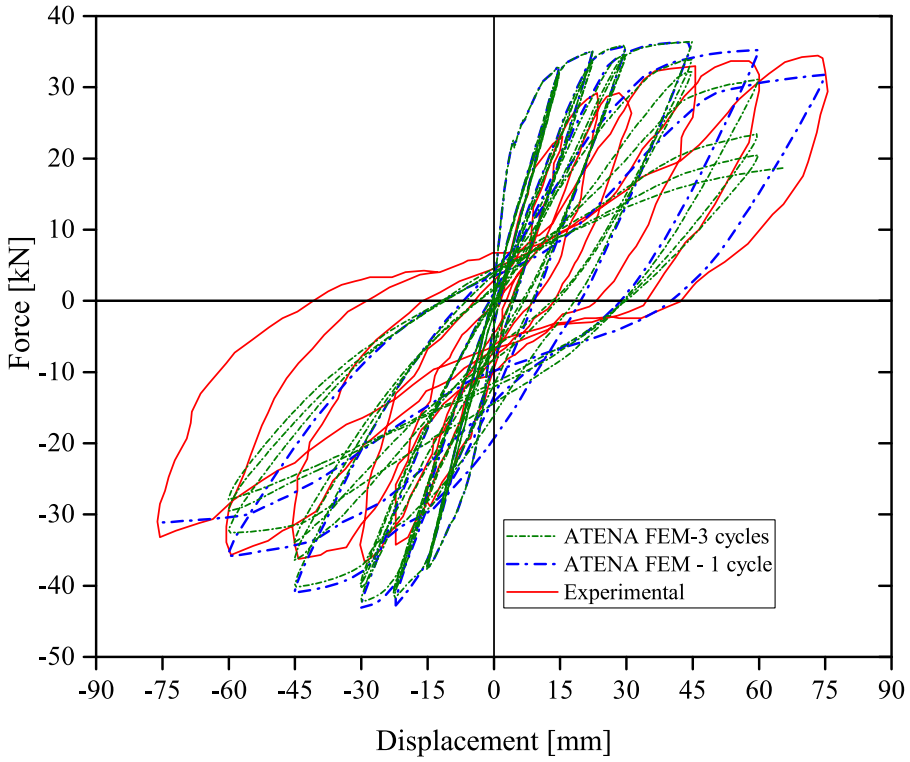

Fig. 14. Comparison between the first cycles of each displacement step of the experimental curve of the beam–column joint without retrofit (CJ2), and the curves obtained from the numerical analysis with one and three cycles for step.

- The numerical hysteresis curves show that, with positive displacements, the force in the column has a trend almost constant after yielding, while, for negative displacements, the force decreases when the displacement increases as it is shown by the experimental curves. In addition, it can be observed that the pinching effect obtained in the experimental test is reproduced by the numerical model.
- As regards the prediction of the peak shear load in the column, V_c, the numerical model using one cycle provides a value of 34.9 kN at an horizontal displacement of 45 mm, while in the experimental test, the maximum load is 34.7 kN at an horizontal displacement of 75 mm. Although the maximum loads are reached at different displacements, their values are very close, in fact, the percentage difference is only of 0.6%.

By considering Fig. 15, similar observations can be made also for the numerical model of the RC BCJ retrofitted with the HPFRC jacket (RCJ2).

As regards the prediction of the peak shear load in the column, V_c, the numerical model provides a value of 45 kN at an horizontal displacement of 15 mm, while, in the experimental test, the maximum load is 49.5 kN at a horizontal displacement of 22.5 mm, resulting in a percentage load difference of 9.1%.

Since the ability of the numerical model to predict the maximum load is satisfying, it can be deduced that the chosen interface relationship can well represent the real interaction between concrete and UHPFRC, when adequate values of the relationship parameters are used.

On the basis of the observations made about the two implemented numerical models, it can be said that they simulate RC exterior BCJs behavior under cyclic loads sufficiently accurately, especially for the prediction of the maximum load, which is the main parameter of interest to verify the joint strength. This allows the use of the numerical models to determine the acting shear force in BCJs.

In Fig. 15 also the shear load in the column, calculated through the analytical formulation (Eq. (59)), is shown. Since the considered specimens were subjected to beam flexural failure, the shear on the beam at failure, V_b, required by Eq. (59) is calculated dividing the beam resisting bending moment, obtained from the flexural model (Eq. (37)), by the beam length. The shear acting on the column obtained by Eq. (59) is equal to 49.99 kN, which presents a percentage difference of 0.8% compared to the experimental result.

Table 7 summarizes the shear load values in the column obtained by the experimental tests and the analytical and numerical models for both the considered specimens. From this table it can be concluded that both analytical and numerical models predict very well the maximum load on the column at the beam flexural failure. In particular, the proposed analytical model is the most accurate. This is a further validation of the proposed flexural model. It is stressed that the shear force in the column, calculated as described above, is the maximum one, because, after the beam flexural failure, shear in the column cannot increase any more. This value of shear is not reached if shear failure occurs in the joint before the beam flexural failure. Knowing the joint shear strength from the shear model (Eq. (56)) and comparing this value with the maximum joint shear force, obtained from Eq. (57), at the

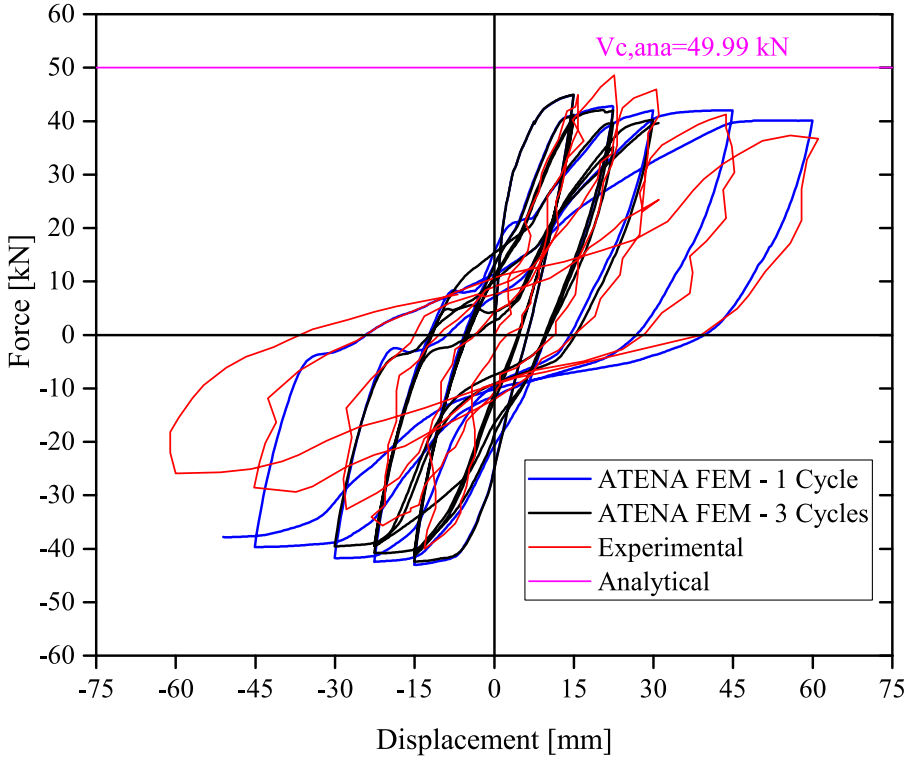

Fig. 15. Comparison between the first cycles of each displacement step of the experimental curve of the beam–column joint retrofitted with HPFRC (RCJ2) and the curve obtained from the numerical analysis with three cycles for step.

Table 7
Values of the shear load in the column (V_c) obtained from the experimental test and the analytical and numerical models, and comparisons.

Specimen	Exp [kN]	Ana. [kN]	FEM [kN]	Error [%] Exp/Ana	Error [%] Exp/FEM
CJ2	34.7	–	34.9	–	0.6
RCJ2	49.5	49.9	45.0	0.8	9.1

beam flexural failure, it is possible to establish if joint shear failure can occur or not. In this sense, the proposed flexural model, from which the maximum joint shear force can be derived, and the shear model, which provides the joint shear strength, appear as valuable tools for researchers and engineers to establish which type of failure will occur in BCJs retrofitted with UHPFRC jacket. If shear failure results from the design of the retrofitted joint, it is possible to avoid this failure by increasing the UHPFRC jacket thickness until flexural failure occurs instead of shear one.

5. Conclusions

The behavior of exterior RC BCJs retrofitted with UHPFRC jacket under cyclic lateral loads has been investigated herein. An analytical flexural model, which allows the calculation of the beam ultimate bending moment has been proposed, to determine the joint shear force at beam flexural failure. An analytical shear model to calculate the joint shear strength has been provided to assess if joint shear failure occurs. Also, a numerical model of an exterior BCJ retrofitted with UHPFRC jacket is provided. On the basis of the performed analyses the following conclusions are drawn.

1. The analytical flexural model is able to accurately predict the ultimate bending moment of beams strengthened by a UHPFRC jacket. For the considered set of specimens, the model provides estimates with an absolute percentage error lower than 9%.
2. For the considered specimens, which show beam flexural failure, the analytical shear model provides joint shear strength predictions greater than the maximum joint shear force, correspondently to the experimental evidences. Moreover, the shear strength of the diagonal concrete strut is always greater than the maximum shear force acting in the strut.
3. The shear model shows that the UHPFRC jacket applied to exterior BCJs significantly increases both the maximum shear force acting in the joint core, due to the increase of stiffness of the confined concrete, and the joint shear strength, thanks to the shear strength contribution of the jacket. A percentage contribution of the UHPFRC jacket to the joint strength up to 67.2% is obtained.
4. The confinement effect produced by the UHPFRC jacket on the concrete diagonal strut in the joint core, considered in the shear model, increases the compressive strength of the concrete diagonal strut. An increase up to about 32% is observed for the considered specimens.
5. Engineers can easily use the flexural model to calculate the maximum shear force on BCJ retrofitted with UHPFRC jacket at beam flexural failure, and the shear model to calculate the joint shear strength. In this way, it is possible to evaluate whether the beam flexural failure or the joint shear failure occurs. Based on the obtained result, it is possible to establish if the thickness of the UHPFRC jacket is adequate to avoid shear failure, which is an unwanted brittle failure mechanism.
6. The numerical methodology used to reproduce the experimental behavior of two RC BCJs, non-retrofitted and retrofitted with HPFRC jacket, shows a good accuracy in the prediction of the experimental results, with a percentage difference of 0.6% and 9.1% in the column shear force, respectively. Hence it can be gathered that the proposed methodology, and in particular the interface interaction relationship used to reproduce the contact between concrete and HPFRC, is suitable to reproduce the experimental results.

Table A.1
Analytical equations for strains and stresses in Cases 1, 2 and 3.

Case 1 ($x_c < \delta_R$)		Case 2 ($\delta_R < x_c < \delta_R + d'$)		Case 3 ($x_c > \delta_R + d'$)	
$\epsilon_{cuR} = \frac{\epsilon_{ut1}}{H-x_c} x_c$	(1)	As case 1		As Case 1	
$\epsilon_{ut'} = \frac{\epsilon_{ut1}}{H-x_c}(\delta_R - x_c)$	(2)	$\epsilon_{ut'} = \epsilon_{ut''}$ (Case 1)		As case 2	
$\epsilon_{ut''} = \frac{\epsilon_{ut1}}{H-x_c}(H - x_c - \delta_R)$	(3)	Not present		Not present	
$\epsilon_{sc} = \frac{\epsilon_{ut1}}{H-x_c}(H - x_c - \delta_R - d')$	(4)	As Case 1		As Case 1	
$\epsilon_{sc'} = \frac{\epsilon_{ut1}}{H-x_c}(\delta_R - x_c + d')$	(5)	As Case 1		$\epsilon_{sc'} = \frac{\epsilon_{ut1}}{H-x_c}(x_c - \delta_R - d')$	(6)
$y = \frac{\epsilon_{ut,crack}}{\epsilon_{ut1}}(H - x_c)$	(7)	As Case 1		As Case 1	
$f_{ut'} = f_{ut} + \frac{f_{ut1}-f_{ut}}{\epsilon_{ut1}-\epsilon_{ut,crack}}(\epsilon_{ut'} - \epsilon_{ut,crack})$	(8)	As Case 1		As Case 1	
$f_{ut''} = f_{ut} + \frac{f_{ut1}-f_{ut}}{\epsilon_{ut1}-\epsilon_{ut,crack}}(\epsilon_{ut''} - \epsilon_{ut,crack})$	(9)	Not present		Not present	
Not present		$C_c = \beta_c(x_c - \delta_R) f_c \alpha_c b$	(10)	As Case 2	
$C_{R1} = \beta_R \delta_R \alpha_R f_{cR} B$	(11)	$C_{R1} = \delta_R \alpha_R f_{cR} B$	(12)	As Case 2	
Not present		$C_{R2} = (\beta_R x_c - \delta R)\alpha_R f_{cR} 2\delta_R$	(13)	As Case 2	
$T_{R1} = \frac{f_{ut} y}{2} B$	(14)	$T_{R1} = f_{ut} y \delta_R$	(15)	As Case 2	
$T_{R2} = \frac{f_{ut}-f_{ut'}}{2}(\delta_R - x_c - y)B$	(16)	$T_{R2} = (f_{ut} - f_{ut'})(H - \delta_R - x_c - y)\delta_R$	(17)	As Case 2	
$T_{R3} = f_{ut'}(\delta_R - x_c - y)B$	(18)	$T_{R3} = f_{ut'}(H - \delta_R - x_c - y)2\delta_R$	(19)	As Case 2	
$T_{R4} = (f_{ut'} - f_{ut''})(H - 2\delta_R)\delta_R$	(20)	$T_{R4} = \frac{f_{ut}-f_{ut1}}{2}\delta_R B$	(21)	As Case 2	
$T_{R5} = f_{ut''}(H - 2\delta_R)2\delta_R$	(22)	$T_{R5} = f_{ut1}\delta_R B$	(23)	As Case 2	
$T_{R6} = \frac{f_{ut''}-f_{ut1}}{2}\delta_R B$	(24)	Not present		Not present	
$T_{R7} = f_{ut1}\delta_R B$	(25)	Not present		Not present	
$C_{sc} = \epsilon_{sc} E_s A_{sc} \leq A_{sc} f_{sy}$	(26)	As Case 1		As Case 2	
$C_{sc'} = \epsilon_{sc'} E_s A_{sc'} \leq A_{sc'} f_{sy}$	(27)	As Case 1		As Case 2	

7. The main advantage of the proposed model is the direct calculation of the joint shear strength to be used for the UHPFRC jacket design to avoid brittle joint shear failure.
8. Finally, it has to be stressed that due to the current lack of experimental tests on BCJs retrofitted with UHPFRC jacket, more experimental data should be collected in the future to further corroborate the accuracy of the proposed formulas.

CRediT authorship contribution statement

Ingrid Rocio Irreño Palomo: Writing – original draft, Visualization, Validation, Software, Investigation, Formal analysis, Data curation. **Giada Frappa:** Writing – review & editing, Methodology, Formal analysis, Conceptualization. **Luiz Carlos de Almeida:** Supervision, Project administration, Funding acquisition. **Leandro Mouta Trautwein:** Supervision, Software, Formal analysis. **Margherita Pauletta:** Writing – review & editing, Supervision, Resources, Methodology, Conceptualization.

Declaration of competing interest

The authors declare the following financial interests/personal relationships which may be considered as potential competing interests: Margherita Pauletta reports financial support was provided by European Union Next-GenerationEU, NATIONAL RECOVERY AND RESILIENCE PLAN (PNRR), MISSION 4 COMPONENT 2, INVESTMENT 1.5, within the Interconnected Nord-Est Innovation Ecosystem (iNEST). Giada Frappa reports financial support was provided by European Union Next-GenerationEU, NATIONAL RECOVERY AND RESILIENCEPLAN (PNRR), MISSION 4 COMPONENT 2, INVESTMENT 1.5, within the Interconnected Nord-EstInnovation Ecosystem (iNEST). Ingrid Rocio Irreno Palomo reports financial support was provided by Brazilian National Council for Scientific and Technological Development (CNPq). Ingrid Rocio IrrenoPalomo reports financial support was provided by Personnel Improvement Coordination Higher Education - Brazil (CAPES). Nothing to declare. If there are other authors, they declare that they have no known competing financial interests or personal relationships that could have appeared to influence the work reported in this paper.

Data availability

No data was used for the research described in the article.

Acknowledgments

This work was supported by the Brazilian National Council for Scientific and Technological Development (CNPq) (Grant No. 141517/2021-2). This study was financed in part by the Coordenação de Aperfeiçoamento de Pessoal de Nível Superior - Brasil (CAPES) - Finance Code 001. This work also was partially funded by the European Union Next-GenerationEU (PIANO NAZIONALE DI RIPRESA E RESILIENZA (PNRR) – MISSIONE 4 COMPONENTE 2, INVESTIMENTO 1.5 – D.D. 1058 23/06/2022, ECS00000043), within the Interconnected Nord-Est Innovation Ecosystem (iNEST). This manuscript reflects only the authors' views and opinions, neither the European Union nor the European Commission can be considered responsible for them. This work was also partially funded by the strategic plan of University of Udine within the framework of the project "ESPeRT", whose support is greatly appreciated.

Annex

See Table A.1.

References

[1] Frappa G, Pauletta M. Seismic retrofitting of a reinforced concrete building with strongly different stiffness in the main directions. In: Proceedings of the 14th fib international PhD symposium in civil engineering, Rome, Italy. 2022.
[2] Di Marco C, Frappa G, Sabbà MF, Campione G, Pauletta M. Shear strength formula for interior beam–column joints with plain bars in existing buildings. Eng Struct 2023;293:116656. http://dx.doi.org/10.1016/j.engstruct.2023.116656.
[3] Karayannis CG, Chalioris CE, Sideris KK. Effectiveness of RC beam–column connection repair using epoxy resin injections. J Earthq Eng 1998;2(2):217–40. http://dx.doi.org/10.1080/13632469809350320.
[4] Karayannis CG, Chalioris CE, Sirkelis GM. Local retrofit of exterior RC beam–column joints using thin RC jackets—An experimental study. Earthq Eng Struct Dyn 2008;37(5):727–46.
[5] Noyan MMA. Experimental study on the behavior of RC beam–column joint retrofitted with ferrocement jacket under cyclic loading. 2014.
[6] Li S, Li Q, Jiang H, Zhang H, Zhang L. Experimental research on seismic performance of a new-type of R/C beam–column joints with end plates. Shock Vib 2017;1–11. http://dx.doi.org/10.1155/2017/3823469.
[7] Ebanesar A, Gladston H, Farsangi EN, Sharma SV. Strengthening of RC beam–column joints using steel plate with shear connectors: Experimental investigation. Structures 2022;35:1138–50. http://dx.doi.org/10.1016/j.istruc.2021.08.042.
[8] Said A, Nehdi M. Rehabilitation of RC frame joints using local steel bracing. Struct Infrastruct Eng 2008;4(6):431–47. http://dx.doi.org/10.1016/j.istruc.2021.08.042.

[9] Mukherjee A, Joshi M. FRPC reinforced concrete beam–column joints under cyclic excitation. Compos Struct 2005;70(2):185–99. http://dx.doi.org/10.1016/j.compstruct.2004.08.022.

[10] Pampanin S, Bolognini D, Pavese A. Performance-based seismic retrofit strategy for existing reinforced concrete frame systems using fiber-reinforced polymer composites. J Compos Constr 2007;11(2):211–26. http://dx.doi.org/10.1061/(asce)1090-0268(2007)11:2(211).

[11] Beydokhty EZ, Shariatmadar H. Behavior of damaged exterior RC beam–column joints strengthened by CFRP composites. Lat Am J Solids Struct 2016;13:880–96. http://dx.doi.org/10.1590/1679-78252258.

[12] Ma C, Wang D, Wang Z. Seismic retrofitting of full-scale RC interior beam–column-slab subassemblies with CFRP wraps. Compos Struct 2017;159:397–409. http://dx.doi.org/10.1016/j.compstruct.2016.09.094.

[13] Pohoryles DA, Melo J, Rossetto T, D'Ayala D, Varum H. Experimental comparison of novel CFRP retrofit schemes for realistic full-scale RC beam–column joints. J Compos Constr 2018;22(5):04018027. http://dx.doi.org/10.1061/(asce)cc.1943-5614.0000865.

[14] Obaidat YT, Abu-Farsakh GA, Ashteyat AM. Retrofitting of partially damaged reinforced concrete beam–column joints using various plate-configurations of CFRP under cyclic loading. Constr Build Mater 2019;198:313–22. http://dx.doi.org/10.1016/j.conbuildmat.2018.11.267.

[15] Ilia E, Mostofinejad D, Moghaddas A. Cyclic behavior of strong beam–weak column joints strengthened with different configurations of CFRP sheets. Arch Civ Mech Eng 2020;20:1–26. http://dx.doi.org/10.1007/s43452-020-0015-7.

[16] Lee WT, Chiou YJ, Shih MH. Reinforced concrete beam–column joint strengthened with carbon fiber reinforced polymer. Compos Struct 2010;92(1):48–60. http://dx.doi.org/10.1016/j.compstruct.2009.06.011.

[17] Attari N, Amziane S, Chemrouk M. Efficiency of beam–column joint strengthened by FRP laminates. Adv Compos Mater 2010;19(2):171–83. http://dx.doi.org/10.1163/092430409X12605406698192.

[18] Parvin A, Altay S, Yalcin C, Kaya O. CFRP rehabilitation of concrete frame joints with inadequate shear and anchorage details. J Compos Constr 2010;14(1):72–82. http://dx.doi.org/10.1061/(asce)cc.1943-5614.0000055.

[19] Ilki A, Bedirhanoglu I, Kumbasar N. Behavior of FRP-retrofitted joints built with plain bars and low-strength concrete. J Compos Constr 2011;15(3):312–26. http://dx.doi.org/10.1061/(asce)cc.1943-5614.0000156.

[20] Sezen H. Repair and strengthening of reinforced concrete beam–column joints with fiber-reinforced polymer composites. J Compos Constr 2012;16(5):499–506. http://dx.doi.org/10.1061/(asce)cc.1943-5614.0000290.

[21] Choudhury AM, Deb SK, Dutta A. Study on size effect of fibre reinforced polymer retrofitted reinforced concrete beam–column connections under cyclic loading. Can J Civil Eng 2013;40(4):353–60. http://dx.doi.org/10.1139/cjce-2012-0041.

[22] Realfonzo R, Napoli A, Pinilla JGR. Cyclic behavior of RC beam–column joints strengthened with FRP systems. Constr Build Mater 2014;54:282–97. http://dx.doi.org/10.1016/j.conbuildmat.2013.12.043.

[23] Del Vecchio C, Di Ludovico M, Balsamo A, Prota A, Manfredi G, Dolce M. Experimental investigation of exterior RC beam–column joints retrofitted with FRP systems. J Compos Constr 2014;18(4):04014002. http://dx.doi.org/10.1061/(asce)cc.19435614.0000459.

[24] Shannag MJ, Alhassan MA. Seismic upgrade of interior beam–column subassemblages with high-performance fiber-reinforced concrete jackets. ACI Struct J 2005;102(1):131–8. http://dx.doi.org/10.14359/13538.

[25] Shannag MJ, Barakat S, Abdul-Kareem M. Cyclic behavior of HPFRC-repaired reinforced concrete interior beam–column joints. Mater Struct 2002;35:348–56.

[26] Beschi C, Riva P, Metelli G, Meda A. HPFRC jacketing of non seismically detailed RC corner joints. J Earthq Eng 2015;19(1):25–47. http://dx.doi.org/10.1080/13632469.2014.948646.

[27] Khan MI, Al-Osta MA, Ahmad S, Rahman MK. Seismic behavior of beam–column joints strengthened with ultra-high performance fiber reinforced concrete. Compos Struct 2018;200:103–19. http://dx.doi.org/10.1016/j.compstruct.2018.05.080.

[28] Sharma R, Bansal P. Behavior of RC exterior beam column joint retrofitted using UHP-HFRC. Constr Build Mater 2019;195:376–89. http://dx.doi.org/10.1016/j.conbuildmat.2018.11.052.

[29] Saharan S, Kaur G, Bansal PP. Confined UHPFRC for retrofitting of RC beam–column joint: An experimental study. Mag Concr Res 2023;75(5):217–33.

[30] Al-Osta MA, Isa MN, Baluch MH, Rahman MK. Flexural behavior of reinforced concrete beams strengthened with ultra-high performance fiber reinforced concrete. Constr Build Mater 2017;134:279–96. http://dx.doi.org/10.1016/j.conbuildmat.2016.12.094.

[31] Isa MN. Flexural improvement of plain concrete beams strengthened with high performance fibre reinforced concrete. Niger J Technol 2017;36(3):697–704. http://dx.doi.org/10.4314/njt.v36i3.6.

[32] Ji H, Liu C. Ultimate shear resistance of ultra-high performance fiber reinforced concrete-normal strength concrete beam. Eng Struct 2020;203:109825. http://dx.doi.org/10.1016/j.engstruct.2019.109825.

[33] Sakr MA, Sleemah AA, Khalifa TM, Mansour WN. Behavior of RC beams strengthened in shear with ultra-high performance fiber reinforced concrete (UHPFRC). In: MATEC web of conferences. vol. 199, 2018, http://dx.doi.org/10.1051/matecconf/201819909002.

[34] Safdar M, Matsumoto T, Kakuma K. Flexural behavior of reinforced concrete beams repaired with ultra-high performance fiber reinforced concrete (UHPFRC). Compos Struct 2016;157:448–60. http://dx.doi.org/10.1016/j.compstruct.2016.09.010.

[35] Tanarslan HM. Flexural strengthening of RC beams with prefabricated ultra high performance fibre reinforced concrete laminates. Eng Struct 2017;151:337–48. http://dx.doi.org/10.1016/j.engstruct.2017.08.048.

[36] Garg V, Bansal PP, Sharma R. Retrofitting of shear-deficient RC beams using UHP-FRC. Iran J Sci Technol, Trans Civ Eng 2019;43:419–28. http://dx.doi.org/10.1007/s40996-019-00241-7.

[37] Sakr MA, Sleemah AA, Khalifa TM, Mansour WN. Shear strengthening of reinforced concrete beams using prefabricated ultra-high performance fiber reinforced concrete plates: Experimental and numerical investigation. Struct Concr 2019;20(3):1137–53. http://dx.doi.org/10.1002/suco.201800137.

[38] Lampropoulos AP, Paschalis SA, Tsioulou OT, Dritsos SE. Strengthening of reinforced concrete beams using ultra high performance fibre reinforced concrete (UHPFRC). Eng Struct 2016;106:370–84. http://dx.doi.org/10.1016/j.engstruct.2015.10.042.

[39] Hussein L, Amleh L. Structural behavior of ultra-high performance fiber reinforced concrete-normal strength concrete or high strength concrete composite members. Constr Build Mater 2015;93:1105–16. http://dx.doi.org/10.1016/j.conbuildmat.2015.05.030.

[40] Anusree K. Study on strengthening of RC beams overlaying with UHPFRC. Int J Appl Eng Res 2019;14(12). (Special Issue), ©Research India Publications. http://www.ripublication.com.

[41] Chen RP, Ma QL, Zhang Y, Wu HN, Liu Y, Lu L. Experimental study on the mechanical behaviour of eccentric compression short column strengthened by ultra-high-performance fibre-reinforced concrete. Structures 2021;33:508–22. http://dx.doi.org/10.1016/j.istruc.2021.04.078.

[42] Menna C, Mazia C, Sgobba S, Asprone D, Prota A. Structural behavior of strengthened RC columns using high performance fiber reinforced concrete. In: 4th international conference symposium on ultra high performance concrete and high performance construction materials. 2016, p. 9–11.

[43] Cassese P, Menna C, Occhiuzzi A, Asprone D. Experimental behavior of existing RC columns strengthened with HPFRC jacket under concentric and eccentric compressive load. Buildings 2021;11(11). http://dx.doi.org/10.3390/buildings11110521.

[44] Elsayed M, Tayeh BA, Abou Elmaaty M, Aldahshoory Y. Behaviour of RC columns strengthened with Ultra-High Performance Fiber Reinforced concrete (UHPFRC) under eccentric loading. J Build Eng 2023;47:1–35. http://dx.doi.org/10.1016/j.jobe.2021.103857.

[45] Huang Y, Grünewald S, Schlangen E, Luković M. Strengthening of concrete structures with ultra high performance fiber reinforced concrete (UHPFRC): A critical review. Constr Build Mater 2022;336:127398. http://dx.doi.org/10.1016/j.conbuildmat.2022.127398.

[46] Naaman AE, Reinhardt HW. Characterization of high-performance fiber reinforced cement composites—HPFRCC. High-perform Fiber Reinf Cem Compos 1996;2:1–24.

[47] Wille K, El-Tawil S, Naaman AE. Properties of strain hardening ultra-high performance fiber reinforced concrete (UHP-FRC) under direct tensile loading. Cem Concr Compos 2014;48:53–66. http://dx.doi.org/10.1016/j.cemconcomp.2013.12.015.

[48] Association Française de Génie Civil (AFGC)/ Service d'études techniques des routes et autoroutes (SETRA), Bétons fibrés à ultra-hautes performances. 2002, Recommandations provisoires.

[49] French Standard Institute. National addition to Eurocode 2 – Design of concrete structures: specific rules for Ultra-High Performance Fibre-Reinforced Concrete (UPHFRC), NF P 18-710, France. 2016.

[50] Sohail M, Kahraman R, Al Nuaimi N, Gencturk B, Alnahhal W. Durability characteristics of high and ultra-high performance concretes. J Build Eng 2021;33:101669.

[51] Afroughsabet V, Biolzi L, TOzbakkaloglu T. High-performance fiber-reinforced concrete: a review. J Mater Sci 2016;51:6517–51.

[52] Kaïkea A, Achoura D, Duplan F, Rizzuti L. Effect of mineral admixtures and steel fiber volume contents on the behavior of high performance fiber reinforced concrete. Mater Des 2014;63:493–9.

[53] Walraven J. High performance fiber reinforced concrete: progress in knowledge and design codes. Mater Struct 2009;42(9):1247–60.

[54] Naaman A, Reinhardt HW. Proposed classification of HPFRC composites based on their tensile response. Mater Struct 2006;39:547–55.

[55] Park S, Kim D, Ryu G, Koh K. Tensile behavior of ultra high performance hybrid fiber reinforced concrete. Cem Concr Compos 2012;34(2):172–84.

[56] Bahraq AA, Al-Osta MA, Khan MI, Ahmad S. Numerical and analytical modeling of seismic behavior of beam–column joints retrofitted with ultra-high performance fiber reinforced concrete. Structures 2021;32:1986–2003. http://dx.doi.org/10.1016/j.istruc.2021.04.004.

[57] Joint ACI-ASCE Committee 352. Recommendations for design of beam-column connections in monolithic reinforced concrete structures (ACI 352R-02). Farmington Hills, MI: American Concrete Institute; 2002.

[58] Sakr MA, El Korany TM, Osama B. Analysis of RC columns strengthened with ultra-high performance fiber reinforced concrete jackets under eccentric loading. Eng Struct 2020;220:111016. http://dx.doi.org/10.1016/j.istruc.2021.04.004.
[59] Fayaz Q, Kaur G, Bansal PP. Numerical modelling of seismic behaviour of an exterior RC beam column joint strengthened with UHPFRC and CFRP. Arab J Sci Eng 2022;47:4791–896. http://dx.doi.org/10.1007/s13369-021-06334-8.
[60] V. Červenka, L. Jendele, J. Červenka. ATENA program documentation Part 1: Theory. Červenka consulting. 2021.
[61] Palomo IRI, Martínez JDJ, Benedetty CA, Almeida LCD, Trautwein LM, Krahl PA. Prediction of the ultimate capacity of reinforced concrete elements using nonlinear analysis methodologies. Revista IBRACON Estruturas Mater 2023;17:e17210.
[62] Habel K, Denarié E, E. Brühwiler. Structural response of elements combining ultrahigh-performance fiber-reinforced concretes and reinforced concrete. J Struct Eng 2006.
[63] Paschalis S, Lampropoulos A. Developments in the use of Ultra High Performance Fiber Reinforced Concrete as strengthening material. Eng Struct 2021;233:111914.
[64] Huang Y, Grünewald S, Schlangen E, Lukovic M. Strengthening of concrete structures with ultra high performance fiber reinforced concrete (UHPFRC): A critical review. Constr Build Mater 2013;40:50–9.
[65] Nagib M, Sakr M, El-khoriby S, Khalifa T. Interfacial shear behavior between UHPFRC layers and normal concrete substrate for shear-strengthened squat RC shear walls under cyclic loading. Eng Struct 2022;254:113850.
[66] Al Osta M, Khan M, Bahraq A, Xu S. Application of ultra-high performance fiber reinforced concrete for retrofitting the damaged exterior reinforced concrete beam–column joints. Earthq Struct 2020;19(5):361–77.
[67] Mertol HC, Rizkalla S, Zia P, Mirmiran A. Characteristics of compressive stress distribution in high-strength concrete. ACI Struct J 2008;105(5):626.
[68] ACI Committee 318. ACI 318-19: Building code requirements for structural concrete and commentary. 2019.
[69] NTC18 Decreto ministeriale 20/2/2018: norme tecniche delle costruzioni. Ministero delleinfrastrutture e dei trasporti, S.O. (No. 8) alla G.U. No. 42 del 20/2/2018, Ministero delleInfrastrutture e dei Trasporti, Rome, Italy. 2018, (in Italian).
[70] BSI. BS EN 1992-1-1: Eurocode 2: design of concrete structures, Part 1–1: General rules and rules for buildings. London, UK: European Committee for Standardization: British Standards Institution, BSI; 2004.
[71] Samani AK, Attard MM. Lateral strain model for concrete under compression. ACI Struct J 2014;111(2):441–51. http://dx.doi.org/10.14359/51686532.
[72] Pauletta M, Di Luca D, Russo G. Exterior beam column joints–shear strength model and design formula. Eng Struct 2015;94:70–81. http://dx.doi.org/10.1016/j.engstruct.2015.03.040.
[73] Guo W, Fan W, Shao X, Shen D, Chen B. Constitutive model of ultra-high-performance fiber-reinforced concrete for low-velocity impact simulations. Compos Struct 2018;185:307–26. http://dx.doi.org/10.1016/j.compstruct.2017.11.022.
[74] Russell HG, Graybeal BA, Russell HG. Ultra-high performance concrete: A state-of-the-art report for the bridge community (No. FHWA-HRT-13-060). United States. Federal Highway Administration. Office of Infrastructure Research and Development; 2013.
[75] J.G. Van Mier. Multiaxial strain-softening of concrete, part I: fracture. Mater Struct 1986;19(111).
[76] Menetrey, William. Triaxial failure criterion for concrete and its generalization. ACI Struct J 1995;92(3):311–8, http://dx.doi.org/10.14359/1132.
[77] Hordijk DA. Local approach to fatigue of concrete. [Ph.D. dissertation], Dept. Civil Eng. Delft Univ. Technol; 1991.
[78] JSCE. Standard specifications for concrete structures-2007, design. Tokyo, Japan: Japan Society of Civil Engineers (JSCE); 2007.
[79] Comité Euro-International du Béton, Fédération Internationale du Béton, fib Model Code for Concrete Structures 2010, CEB-FIB 2010. 2010.
[80] M. Menegotto, Pinto PE. Method of analysis for cyclically loaded R. C. plane frames. Including changes in geometry and non-elastic behavior of elements under combined normal force and bending. In: Proceedings of IABSE. Symposium on resistance and ultimate deformability of structures acted on by well defined loads. 1973, p. 15–22.
[81] Paschalis S, Lampropoulos A, Tsioulou O. Experimental and numerical study of the performance of ultra high performance fiber reinforced concrete for the flexural strengthening of full scale reinforced concrete members. Constr Build Mater 2018;186:351–66. http://dx.doi.org/10.1016/j.conbuildmat.2018.07.123.
[82] Sasmal S, Novák B, Ramanjaneyulu K. Numerical analysis of fiber composite-steel plate upgraded beam–column sub-assemblages under cyclic loading. Compos Struct 2011;93:599–610, https://doi.10.1016/j.compstruct.2010.08.019.
[83] Graybeal BA. Material property characterization of ultra-high performance concrete (No. FHWA-HRT-06-103). United States. Federal Highway Administration. Office of Infrastructure Research and Development; 2006.